



저작자표시-비영리-변경금지 2.0 대한민국

이용자는 아래의 조건을 따르는 경우에 한하여 자유롭게

- 이 저작물을 복제, 배포, 전송, 전시, 공연 및 방송할 수 있습니다.

다음과 같은 조건을 따라야 합니다:



저작자표시. 귀하는 원저작자를 표시하여야 합니다.



비영리. 귀하는 이 저작물을 영리 목적으로 이용할 수 없습니다.



변경금지. 귀하는 이 저작물을 개작, 변형 또는 가공할 수 없습니다.

- 귀하는, 이 저작물의 재이용이나 배포의 경우, 이 저작물에 적용된 이용허락조건을 명확하게 나타내어야 합니다.
- 저작권자로부터 별도의 허가를 받으면 이러한 조건들은 적용되지 않습니다.

저작권법에 따른 이용자의 권리는 위의 내용에 의하여 영향을 받지 않습니다.

이것은 [이용허락규약\(Legal Code\)](#)을 이해하기 쉽게 요약한 것입니다.

[Disclaimer](#)

의학박사 학위논문

대사성질환 완화에 관여하는
PPAR γ /AMPK 이중 작용제의 효능
분석에 관한 연구

**Characterization of a Novel
PPAR γ /AMPK Dual Agonist Having
Beneficial Effects on Metabolic Disorder**

2016 년 2 월

서울대학교 대학원
의과학과 의과학전공
최진우

**Characterization of Novel
PPAR γ /AMPK Dual Agonist Having
Beneficial Effect on Metabolic Disorder**

대사성질환 완화에 관여하는
PPAR γ /AMPK 이중 작용제의 효능
분석에 관한 연구

February 2016

The Department of Biomedical Sciences,

Seoul National University

College of Medicine

Jin Woo Choi

Characterization of Novel PPAR γ /AMPK Dual Agonist Having Beneficial Effect on Metabolic Disorder

대사성질환 완화에 관여하는 PPAR γ /AMPK

이중 작용제의 효능 분석에 관한 연구

지도 교수 이 동 섭

이 논문을 의학박사 학위논문으로 제출함

2015년 10월

서울대학교 대학원

의과학과 의과학전공

최 진 우

최진우의 의학박사 학위논문을 인준함

2016년 1월

위 원 장 _____ (인)

부위원장 _____ (인)

위 원 _____ (인)

위 원 _____ (인)

위 원 _____ (인)

**Characterization of Novel
PPAR γ /AMPK Dual Agonist Having
Beneficial Effect on Metabolic Disorder**

by
Jin Woo Choi

**A thesis submitted to the Department of Biomedical
Sciences in partial fulfillment of the requirements for the
Degree of Doctor of Philosophy in Medical Science
at Seoul National University College of Medicine**

January 2016

Approved by Thesis Committee:

Professor _____ Chairman

Professor _____ Vice chairman

Professor _____

Professor _____

Professor _____

Abstract

Insulin resistance, known as a primary cause of obesity and metabolic disorder, has the close relation with type 2 diabetes, hyperlipidemia, hyperglycemia, high cholesterol, atherosclerosis and cardiovascular disease. Especially, lipid metabolite plays an important role in pathogenesis and progression of insulin resistance. Therefore, control of lipid metabolism is important to improve insulin resistance and metabolic diseases.

Cleistocalyx operculatus is a plant widely distributed in southern Asia, and its water extract is commonly used to relieve heat and to prevent and treat diabetes. 2',4'-dihydroxy-6'-methoxy-3',5'-dimethylchalcone (DMC) is a major compound of the extract and is reported to have anti-tumor, anti-oxidative, and anti-inflammatory effects. However, the underlying mechanism of improvement in diabetes and metabolic diseases has not been elucidated.

To carry out this study, we isolated DMC from *Cleistocalyx operculatus* extract to increasing PPAR γ activity. Compared to rosiglitazone, DMC showed a lower PPAR γ transcriptional activity and 10 times lower binding activity to the PPAR γ LBD. However, fatty acid oxidation rate by DMC was higher than that by rosiglitazone. Interestingly, DMC is useful to inhibit adipocyte differentiation, which is totally different from rosiglitazone.

In addition, DMC increases phosphorylation of AMPK, one of the major targets of diabetes and metabolic diseases. Compared to AICAR and metformin, well-known AMPK activators, DMC could increase AMPK activity, even at much lower concentrations.

Next, DMC was administrated to the high-fat fed mice, and the effects of DMC on insulin resistance were determined. DMC improves insulin resistance as effectively as pioglitazone did. Interestingly, DMC treatment reduced fat tissue and showed weight loss compared to the pioglitazone treatment.

Taken together, these results indicate that, DMC will provide

great help to improve lipid metabolism and insulin resistance without side effects such as obesity.

Keywords: DMC, insulin resistance, type 2 diabetes, TZD, PPAR γ , AMPK

Student Number: 2009-30616

Contents

Abstract

List of figure

Introduction

Materials and methods

Result

Discussion

References

국문 초록

List of figures and Tables

<Table 1> Primers used for Real time PCR

Fig 1. Chromatographic figure of *Cleistocalyx operculatus* extracts

Fig 2. *Cleistocalyx operculatus* extracts enhances transcriptional activity

of PPAR γ

Fig 3. Molecular structure of DMC and rosiglitazone

Fig 4. Purity and quality of DMC isolated from *Cleistocalyx operculatus*

Fig 5. DMC enhances transcriptional activity of PPAR (α , γ and δ)

Fig 6. Dose dependent treatment of DMC enhances transcriptional

activity of PPAR γ

Fig 7. Physical interaction of DMC with PPAR γ LBD domain

Fig 8. Effect of DMC on 3T3-L1 adipocyte differentiation

Fig 9. mRNA expression profile of adipogenesis related gene

Fig 10. Effect of DMC on glucose uptake in rat skeletal muscle cells

Fig 11. Effect of fatty acid oxidation in mouse skeletal muscle cells

**Fig 12. . mRNA expression profile of fatty acid oxidation related
gene**

**Fig 13. Increased fatty acid oxidation by DMC was abolished with AMPK
inhibitor**

Fig 14. Effect of DMC on AMPK phosphorylation in C2C12 myotubes

**Fig 15. Time and dose dependent effect of DMC on AMPK
phosphorylation in C2C12 myotubes**

Fig 16. Effect of DMC on fatty acid oxidation in C2C12 myotubes

Fig 17. Effect of DMC on ADP/AMP ratio change

Fig 18. Cell free AMPK activity assay

Fig 19. Physical interaction of DMC with AMPK $\alpha 1\beta 1\gamma 1$

Fig 20. Additive/synergistic effect of DMC and AICAR

Fig 21. Competition assay of DMC and AICAR to AMPK complex

Fig 22. Induction of fatty acid oxidation by DMC is dependent on AMPK

Fig 23. Suppression of adipogenesis is dependent on AMPK

Fig 24. Body weight change of DMC treated diet induced obese mice

Fig 25. Average daily food and water intake of DMC treated diet induced

obese mice

Fig 26. Effect of DMC on glucose tolerance test in diet induced obese mice

Fig 27. Serum profiles of DMC-treated diet induced obese mice

Fig 28. Average tissue weight of DMC treated diet induced obese mice

Fig 29. Morphological change of epididymal white adipose tissue

Fig 30. DMC increased lipolysis related genes in epididymal white

adipose tissue

Fig 31. DMC increased lipogenesis related genes in epididymal

white adipose tissue

Fig 32. DMC decreased C/EBPs and PPAR γ in epididymal white

adipose tissue

Fig 33. DMC enhances fatty acid oxidation in gastrocnemius muscle

Fig 34. DMC enhances fatty acid oxidation in gastrocnemius muscle

Fig 35. DMC decreased lipid droplet in gastrocnemius muscle tissue

<Introduction>

Cleistocalyx operculatus is a plant widely distributed in Vietnam, China, and some other tropical countries [1]. Its flower bud and leaves have been used as traditional herb tea materials to treat respiratory and gastrointestinal disturbance, and as an anti-inflammatory medicine [2]. Also, its dried flower buds have been used as tonic drinks in southern China for thousands of years [3]. Water extract from *Cleistocalyx operculatus* flower buds shows anti-hyperlipidemic effect [4], cardiogenic effect [5], anti-Alzheimer effect [6], anti-hyperglycemic effect [7, 8], pancreatic islets protecting activity [9].

2',4'-dihydroxy-6'-methoxy-3',5'-dimethylchalcone (DMC) is a major compound of the extract and is reported to have anti-tumor [10-16], anti-drug efflux [17-19], anti-inflammation [1, 9], anti-oxidant [4, 20-22], anti-acute liver injury [23], anti-diarrhea [24, 25], anti-microbe [26, 27], anti-virus [28] effect.

Recently, DMC was demonstrated to facilitate glycemic control by suppression of pancreatic α -amylase and glucose transport in the intestine and protection against the H_2O_2 -induced decrease in basal and glucose-stimulated insulin secretion in pancreatic β -cells [29], by antioxidant and anti-apoptosis by the improvement of mitochondrial function [30]. Besides, DMC has been reported to increase glucose uptake in differentiated 3T3-L1 adipocytes [31].

Obesity is a pathological condition characterize as excessive body weight gain. Since redundant energy is usually stored in the fat tissues, average fat cell size and fat tissue mass increase in obesity. Therefore, obesity is simply and specifically defined as an exclusive increase of “fat” mass. Obesity is often caused by the interaction of one or more causal factors, such as diet, sedentary lifestyle, lack of exercise, genetic defects, medical and psychologic illness, socioeconomic influences, early malnutrition, and infectious agents [32, 33]. Despite such evidence, many clinicians considered obesity to be a self-inflicted condition of little medical significance in the past. The increase of body

fat mass accompanies several metabolic disorders, including insulin resistance, type 2 diabetes, hyperglycemia, hyperlipidemia, and cardiovascular diseases [34]. Furthermore, obese individuals have higher susceptibility to type 2 diabetes, hypertension, and coronary heart disease [35].

Diabetes mellitus is caused by complex interaction of genetic and environmental factors. Type 2 diabetes mellitus is characterized by insulin resistance and impaired beta-cell function. At the beginning of type 2 diabetes, blood insulin levels are elevated to compensate insulin resistance. However, as the disease progresses, insulin secretion deteriorates thereby leading to pancreatic beta-cell death. Asymptomatic type 2 diabetes may be undiagnosed for several years. Long-term complications of type 2 diabetes are renal failure (diabetic nephropathy) [36], vascular disease (coronary artery disease, atherosclerosis) [37], vision loss (diabetic retinopathy) [38], loss of feeling or pain (diabetic neuropathy) [39] and heart failure (diabetic cardiomyopathy) [40].

Since type 2 diabetes is caused by the reduction of insulin sensitivity, the regulation of insulin resistance is important for the treatment of type 2 diabetes. Nowadays, several drugs and compounds, such as thiazolidinedione (TZD), metformin have been used to treat hyperglycemia, hyperlipidemia, and insulin resistance.

In the 1980s, ciglitazone was developed as the first TZD [41-43]. Although ciglitazone was not used as a medication, it was concerned for interest in TZD family as drugs. As a result, troglitazone, the first analogue of ciglitazone, was developed for the market in the middle of the 1990s. Since then, more types of TZDs have been developed and identified (e.g. rosiglitazone and pioglitazone). As TZDs strongly bind to and activate peroxisome proliferator-activated receptor gamma (PPAR γ), they greatly sensitize insulin actions by increasing transcription of the target genes. PPAR γ increases the expression of lipid transport-related proteins including adipocyte fatty acid binding protein (aP2), fatty acid transport protein (FATP), lipoprotein lipase (LPL) and CD36 [44]. By modulating lipid transport, PPAR γ

redistributes lipid from circulation and other peripheral tissues such as liver and skeletal muscle to adipose tissue, thereby reducing lipid contents in the circulation, liver and muscle. In addition, these actions of PPAR γ ultimately lead to improve insulin sensitivity by removing lipotoxicity [44].

However, TZDs have significant disadvantages. The major side-effect of TZDs include an increased risk of heart attack [45], stroke [46], and hepatitis due to severe drug toxicity [47], fluid retention [48] and edema [49], which may aggravate heart failure, and weight gain [50, 51]. Due to its links to hepatotoxicity and idiosyncratic acidosis, troglitazone was removed from the market. Pioglitazone (Actos), France and Germany have suspended its sale after a study suggested the drug could raise the risk of bladder cancer [52]. And despite of rosiglitazone's effectiveness at decreasing blood glucose level in type 2 diabetes mellitus, its use decreased dramatically as studies showed apparent associations with increased risks of heart attacks and death [53]. For these reason, rosiglitazone (Avandia), which

was put under selling restrictions in the USA and withdrawn from the market in Europe due to some studies suggesting an increased risk of cardiovascular events. However, the several report that there is no clinical evidence was raised. Upon re-evaluation of new data in 2013, the FDA lifted the restrictions. Concerns about these adverse effects have decreased TZD prescriptions despite its significant effect on metabolic syndrome. Therefore, the need for new drugs with reduced side effects has increased steadily.

Another therapeutic target for diabetes is AMP-dependent protein kinase (AMPK). AMPK is a serine/threonine protein kinase and functions as a central regulator of whole body energy balance. In general, AMPK promotes catabolic pathways to generate more ATP, and inhibits anabolic pathways. Several studies reveals, AMPK as a metabolic sensor that allows for adaptive changes in growth, differentiation and metabolism under conditions of low energy [54-59]. In most species, AMPK exists as an obligate heterotrimer, containing a catalytic subunit (α), and two regulatory subunits (β and γ). Genes

encoding the three subunits are also readily recognized in the genomes of almost all eukaryotes, from simple single-celled protozoa to humans. Based on genetic studies in lower eukaryotes, the ancestral role of this conserved pathway appears to have been in the response to glucose starvation. The AMPK-signaling pathway represents a mechanism to respond to fluctuating glucose levels that appears to have evolved much earlier than the insulin-signaling pathway, which is only found in multicellular animals. Of particular interest, in the nematode worm *Caenorhabditis elegans* AMPK is required for the extension of life span that is observed in response to caloric restriction or to mutations that reduce the function of the insulin-signaling pathway [60, 61].

Under lowered ATP levels, AMP can directly bind to γ regulatory subunit of AMPK, lead to conformational change that promotes AMPK phosphorylation and also protects AMPK dephosphorylation machinery [62]. Binding of AMP or ADP (but not ATP) to the AMPK γ subunit causes a conformational change that promotes phosphorylation of Thr-172 by upstream kinases while

inhibiting dephosphorylation by upstream phosphatases [63-65]. Stoichiometric phosphorylation of Thr-172 can cause > 100-fold activation, although Thr-172 may only be partially phosphorylated *in vivo* even *in vitro* experiencing metabolic stress. The effect of increased phosphorylation is amplified up to 10-fold further by allosteric activation which is caused only by binding of AMP. This tripartite mechanism means that there can be large increases in AMPK activity in response to small increases in the AMP:ATP or ADP:ATP ratios [66].

In the skeletal muscles, AMPK activation increases insulin-independent glucose uptake, which may be important for overcoming hyperglycemia in the insulin-resistant state [67]. In addition, activation of AMPK increases fatty acid oxidation rate: AMPK phosphorylates and inactivates acetyl-coA carboxylase (ACC), which catalyzes transition of acetyl-CoA to malonyl-CoA. Because malonyl-CoA allosterically inhibits carnitine palmitoyltransferase I (CPT1), which catalyzes the transport of fatty-acyl CoA into the mitochondria, AMPK activation eventually increases fatty acid oxidation (FAO) [68]. There

are many AMPK activators; many of them activate AMPK via an increasing AMP:ATP ratio. However, some activators increase AMPK activity by stimulating T172 phosphorylation or by binding directly to AMPK subunits [69].

In this study, I screened 14 putative PPAR γ agonists from *Cleistocalyx operculatus* extract with PPRE tk luciferase assay. Then I examined whether DMC physically interacted with the PPAR γ LBD domain like rosiglitazone does. However, efficiency in activating PPAR γ was not satisfactory compared to rosiglitazone. I also tested the effect of DMC on the 3T3-L1 adipocyte differentiation. Although, I found that DMC as a ligand of PPAR γ , however, DMC suppressed adipogenesis. Next, I demonstrated that DMC promoted glucose uptake and fatty acid oxidation in myotubes through AMPK phosphorylation. To test whether DMC also effective on skeletal muscle, glucose uptake assay and fatty acid oxidation experiment was performed. To know underlying mechanism, PPAR γ and AMPK inhibitor was co-treated with DMC. Then I examined whether DMC have AMPK

phosphorylation activity. To elucidate how DMC phosphorylates AMPK, I examined ADP/ATP ratio and direct combining DMC with AMPK $\alpha 1\beta 1\gamma 1$ complex protein. To know In vivo effect, DMC was introduce to high fat-fed diet induced obese (DIO) mice. Compared with pioglitazone, I tested insulin resistance and tissue weight and morphology.

In brief, I tried to understand the effect of DMC in vitro and in vivo.

<Materials and Methods>

Plant material

The leaves of *Cleistocalyx operculatus* (Roxb.) Merr and Perry were purchased at the Dong Xuan herbal market, Hanoi, Vietnam, in February 2009 and were identified botanically by Dr. Nguyen Bich Thu, National Institute of Medicinal Materials, Hanoi, Vietnam. A voucher specimen (NIMM2009–05) was deposited at the herbarium of the National Institute of Medicinal Materials, Hanoi, Vietnam.

Extraction and isolation of DMC from *C. operculatus*

The experiment by WK Oh's Lab

DMC isolation method was described previously [28]. In brief, the dried leaves of *C. operculatus* (1.5 kg) were extracted with methanol (3 L \times 2 times) at room temperature for one week. A concentrated crude extract (110 g) was suspended in water (2 L) and partitioned successively with *n*-hexane (2 \times 1.5 L), ethyl acetate (2 \times 1.5 L), and *n*-butanol (2 \times 1.5 L). The partial fraction of ethyl acetate layer (25 g)

was chromatographed over a silica gel column (10 × 30 cm; 63–200 μm particle size) with gradient solvent *n*-hexane/EtOAc (19:1, 18:2...1:19, each 2.5 L) to yield nine fractions (F1-F9) based on the TLC profile. Fraction F3 was further chromatographed over a Sephadex LH-20 column (7 × 40 cm) using MeOH to yield DMC (550 mg). NMR spectra were measured on a Bruker Avance 500 or 600 MHz spectrometer at Seoul National University. HRESIMS were recorded on an Agilent 6530 Q-TOF (Agilent Technologies, Inc., Santa Clara, CA, USA) spectrometer. Silica gel (Merck, 63–200 μm particle size) and RP-18 (Merck, 40–63 μm particle size) were used for column chromatography. TLC was carried out with silica gel 60 F₂₅₄ and RP-18 F₂₅₄ plates. HPLC was carried out using a Gilson system with a UV detector and Optima Pak C₁₈ column (10 × 250 mm, 10 μm particle size, RS Tech, Korea).

LC-MS Analysis

The experiment by WK Oh's Lab

Analysis for purity was performed on an Agilent Series 1100 LC system (Agilent Technologies, Waldbronn, Germany). The LC system was coupled to an Agilent Series 1100 MSD single quadropole (Agilent Technologies) equipped with API-ES source. MS detection was conducted in the scan mode. Samples were separated on a reverse-phase column (INNO C18 column, 150 × 4.6 mm I.D., particle size 5 μ M, 120Å) from Young Jin Biochrom (Sungnam, Korea). The flow rate of the mobile phase was 0.5 mL/min and the injection volume was 10 μ L. 0.1% Formic acid in HPLC water (v/v) (channel A) and acetonitrile (v/v) (channel B) was used as eluenting solvents. The elution gradient was started with 10% solvent B for 5 min, linearly increased B to 100% in 30 min, and held at 100% B for 5 min.

Materials, Plasmids and antibodies

Rosiglitazone, 5-Aminoimidazole-4-carboxamide riboside (AICAR) and Compound C were purchased from Sigma Aldrich (St. Louis, MO,

USA). Metformin (Abcam, Cambridge, UK) and GW9662 (Cayman Chemical, Ann Arbor, MI, USA) were also used. An expression vector expressing mouse PPAR γ (pcDNA-HA-PPAR γ) and the PPRE-TK reporter vector (pPPRE-TK-Luc). Antibodies against pAMPK (phosphorylation at Thr 172 of the α subunit), AMPK, pACC (phosphorylation at Ser 79) and ACC were purchased from Cell Signaling Technology (Danvers, MA, USA), and the antibody against γ -tubulin was from Sigma Aldrich.

Cell culture

3T3-L1 preadipocytes were maintained in Dulbecco's Modified Eagle Medium (DMEM, Hyclone, Logan, UT, USA) supplemented with 10 % calf serum (CS; Gibco, Grand island, NY, USA). Two days after confluence, differentiation of preadipocytes was induced by treatment with DMI [0.25 μ M of dexamethasone (Dex), 0.5 mM of 3-isobutyl- α -methylxanthine (IBMX), and 5 μ g/mL insulin] in DMEM supplemented with 10 % fetal bovine serum (FBS; Gibco, Grand island,

NY, USA). Two days after the induction, the medium was replaced to DMEM supplemented with 10% FBS and 5 µg/mL insulin for additional 2 days. The cells were maintained in DMEM supplemented with 10 % FBS up to 10 days with changing the medium every 2 days. COS7 cells were maintained in DMEM supplemented with 10 % FBS. C2C12 and L6 cells were maintained in DMEM containing 10 % FBS. Myoblast differentiation into myotubes was completed by incubation in DMEM supplemented with 2 % horse serum (HS; Gibco, Grand island, NY, USA) for 5-6 days.

Transient transfection and reporter assays

COS7 cells (5×10^5) were seeded into 12-well plates and transfected with pPPRE-tk-Luc (0.3 µg), pcDNA-HA-PPAR γ (0.1 µg) and pCMV- β -gal (0.1 µg) using Lipofectamin and PLUS reagent (Invitrogen). The cells were treated with DMSO, rosiglitazone (5 µM) or DMC for 24 h. Luciferase activity was determined using the luciferase assay system kit (Promega, Madison, WI, USA) and quantified using GLOMAX

(Promega) according to the manufacturer's instructions. Luciferase activity was normalized by β -galactosidase activity.

Transient transfection of siRNA

3T3-L1 cells or C2C12 cells in 12 well plates were transfected with siAMPK α 1 and α 2 (50nM each) (Dharmacon, Lafayette, CO, USA) using Lipofectamine RNAiMAX (Invitrogen).

Surface plasmon resonance (SPR) spectroscopy

The experiment by Inhee Mook-Jung's Lab

The SPR spectroscopy analysis was performed using a Biacore X-100 (GE Healthcare, Rahway, NJ, USA). The CM5 sensor chip (GE Healthcare) was preactivated by a mixture of N-hydroxysuccinimide and N-ethyl-N'-(dimethylaminopropyl) carbodiimide. PPAR γ LBD (20 mg/ml; Abcam) and AMPK α 1 β 1 γ 1 (20 mg/ml; Abcam) were immobilized separately by N-ethyl-N'-(dimethylaminopropyl) carbodiimide-N-hydroxysuccinimide amine coupling on the CM5

sensor chip. As a control, the same volume of HBS-EP buffer (0.01 mol/L HEPES, pH 7.4, 0.15 mol/L NaCl, 3 mmol/L EDTA, and 0.005% surfactant p20) was applied to the chip surface and the unreacted sites were blocked by injection of ethanolamine. To analyze the binding kinetics, different concentrations of rosiglitazone or DMC diluted in HBS-EP buffer were injected onto the sensor chip of PPAR γ LBD for 540 s at 10 ml/min, and the response unit (RU) was then recorded at 25 $^{\circ}$ C. Similar experiments were performed using DMC and AMP to the sensor chip of AMPK. After injection was stopped, HBS-EP buffer was poured over the chip for 700 s at 10 ml/min to allow the bound analytes to dissociate from the immobilized PPAR γ LBD or AMPK α 1 β 1 γ 1. The RU elicited by injecting HBS-EP buffer alone was used as the control. Biacore X-100 software (GE Healthcare) was used to record the changes in RU and to plot the binding curve. The dissociation equilibrium constant (K_D) to immobilized PPAR γ LBD and AMPK was calculated using kinetic evaluation software. The dissociation equilibrium constant, K_D (M) was obtained by calculating k_d (s^{-1}) / k_a

($M^{-1}s^{-1}$), where k_d and k_a are dissociation- and association-rate constant, respectively. For SPR competition assay, DMC (100 nM) and AMP (100 nM) were injected alone or both into AMPK bounded CM5 sensor chip. To analyze the binding kinetics, response unit (RU) was recorded and plotted as a bar graph.

Measurement of ADP/ATP ratio

ADP and ATP levels were determined by using ADP/ATP ratio Assay Kit (Abcam, Cambridge, UK). The cell content of ATP and ADP was measured according to manufacturer's protocol. Luminescence value was read via a Victor3 1420 multilabel counter (PerkinElmer, Boston, MA, USA).

Cell free AMPK kinase assay

AMPK activity was evaluated by phosphorylation of synthetic SAMS (Abcam, Cambridge, UK) peptide in the absence or presence of different concentration of DMC, as positive control AICAR, metformin

and as negative control Compound C. For cell free AMPK kinase assay, AMPK $\alpha 1\beta 1\gamma 1$ recombinant protein (Abcam, Cambridge, UK) was purchased. Kinase assay were performed in kinase mixture (20 mM Tris-Hcl, 5 mM MgCl₂, 100 mM KCl, 0.1 mM DTT, 100 μ M ATP, 100 μ M AMP, 1 mM EDTA, 0.1 μ g/ μ l AMPK protein, 100 μ M SAMS peptide, and 0.2 μ Ci [γ -³²P] ATP) and incubated at 30 °C for 20 minutes. Reaction mixtures were spotted onto P81 phosphocellulose paper (Whatman, Princeton, NJ, USA) and washed with 1 % phosphoric acid. Radioactivity was determined by liquid scintillation counting.

Measurement of glucose uptake

L6 myotubes were treated with rosiglitazone (5 and 10 μ M), DMC (5 and 10 μ M) for 48 hours. After the addition of insulin (100 nM) to the medium for 30 min, cells were washed with salt-HEPES buffer (4.7 mmol/L KCl, 130 mmol/L NaCl, 1.25 mmol/L CaCl₂, 2.5 mmol/L NaH₂PO₄, 1.2 mmol/L MgSO₄, and 10 mmol/L HEPES). Cells were incubated in salt-HEPES buffer containing 0.2 μ Ci of [³H]

deoxyglucose for 15 min. Uptake was terminated by three rapid washes with cold phosphate-buffered saline (PBS). Cells were lysed using 0.5 mol/L NaOH and neutralized by 1 mol/L HCl. The radioactivity was determined using a Tri-Carb Liquid Scintillation counter (Perkin Elmer, Waltham, MA, USA) and normalized by total protein amount.

Measurement of fatty acid oxidation (FAO)

C2C12 cells were lysed with mitochondria isolation buffer (MIB) buffer (250 mmol/L Sucrose, 20 mmol/L Tris-HCl, pH 7.4, 1 mmol/L EDTA).

The lysates were incubated with FAO reaction buffer (100 mmol/L Sucrose, 10 mmol/L Tris-HCl pH7.4, 5 mmol/L K₂HPO₄, 80 mmol/L KCl, 1mmol/L MgCl₂, 0.1 mmol/L EDTA, 0.1 mmol/L Malate, 1 mmol/L DTT, 0.1 mmol/L NAD, 2 mmol/L ATP, 0.05 mmol/L CoA and 1 mmol/L L-carnitine) containing 0.375 µCi of [¹⁴C] palmitic acid for 2h. ¹⁴CO₂ and ¹⁴C-labeled acid-soluble metabolites were quantified using a liquid scintillation counter and each radioactivity was normalized by protein amount of each lysate.

RNA preparation and real-time PCR

Total RNAs were prepared using TRIzol reagent (Invitrogen) according to the manufacturer's instructions. cDNAs were synthesized by the Reverse Transcription System (Takara, Shiga, Japan). Quantitative real-time PCR (qRT-PCR) was performed with the appropriate primers using SYBR-master mix (Takara) and ABI 7500 real-time PCR system (Applied Biosystems, CA, USA). The 18S rRNA level was used for the internal control. Experiments were performed in duplicate for each sample. Nucleotide sequences of the primers were shown in <Table Fig.

1>

<Table 1> Primers used for Real time PCR

Gene Name	F: forward R: reverse	Sequence (5' to 3')
CD36	F	5'-GGAGGCATTCTCATGCCAGT-3'
	R	5'-CTGCTGTTCTTTGCCACGTC-3'
ACSL1	F	5'-CTGGTTGCTGCCTGAGCTTG-3'
	R	5'-TTGCCCTTTTCACACACACC-3'
CPT1b	F	5'-AAGTGTAGGACCAGCCCCGA-3'
	R	5'-TGCGGACTCGTTGGTACAGG-3'
MCAD	F	5'-TCATTGTGGAAGCCGACACC-3'
	R	5'-GCACCCATTGCGATCTTGAA-3'
PDK4	F	5'-CAATGGCTCAAGGCATCCTG-3'
	R	5'-GCTTGGGTTTCCCGTCTTTG-3'
UCP3	F	5'-AGGAGCCATGGCAGTGACCT-3'
	R	5'-CACAGGCCCTGACTCCTTC-3'
AMPK α 1	F	5'-TGGGGGACACGCTTGGT-3'
	R	5'-GCTTTCCTTTTCGTCCAACCTT-3'
AMPK α 2	F	5'-TGACAGGCCATAAAGTGGCAG-3'
	R	5'-TGTGACAGTAATCCACGGCA-3'
C/EBP β	F	5'-ACCTGGAGACGCAGCACAAG-3'
	R	5'-CTGCTTGAACAAGTCCGCAG-3'
C/EBP δ	F	5'-AAAGTGCAGGCTTGTGGACT-3'
	R	5'-TACTCCACTGCCCACCTGT-3'
C/EBP α	F	5'-GTCGGTGGACAAGAACAGCA-3'
	R	5'-CCTTCTGTTGCGTCTCCACG-3'
PPAR γ	F	5'-TCTGTGGACCTCTCCGTGATGGA-3'
	R	5'-AACCTGATGGCATTGTGAGAC-3'
ATGL	F	5'-GAGCTTCGCGTCACCAAC-3'
	R	5'-CACATCTCTCGGAGGACCA-3'
HSL	F	5'-AGACCACATCGCCCACA-3'
	R	5'-CCTTTATTGTCAGCTTCTTCAAGG-3'

Perilipin	F	5'-CACTCTCTGGCCATGTGGA-3'
	R	5'-AGAGGCTGCCAGGTTGTG-3'
ADD1 SREBP1c	F	5'-GGCCTGCCTGGCACAGAGTG-3'
	R	5'-CTGGGTTCCCGGCCAAGCTG-3'
FASN	F	5'-CGACAGCACCAGCTTCGCCA-3'
	R	5'-CACGCTGGCCTGCAGCTTCT-3'
DGAT	F	5'-CCTCAGCCTTCTTCCATGAG-3'
	R	5'-ACTGGGGCATCGTAGTTGAG-3'
18S rRNA	F	5'-GTAACCCGTTGAACCCATT-3'
	R	5'-CCATCCAATCGGTAGTAGCG-3'

Western blot analysis

Cell lysates were prepared in the lysis buffer containing 20 mmol/L Tris-HCl pH7.4, 1 mmol/L EDTA, 1 mmol/L EGTA, 10 mmol/L $\text{Na}_4\text{P}_2\text{O}_7$ and 2 mmol/L Na_3PO_4 , 1 % TritonX-100, 1 % sodium deoxycholate, 1 % sodium-dodecyl-sulfate (SDS), 150 mmol/L NaCl, 100 mmol/L NaF, supplemented with protease inhibitors [10 $\mu\text{g}/\text{ml}$ aprotinin, 10 $\mu\text{g}/\text{ml}$ leupeptin, and 1 mmol/L phenylmethylsulfonyl fluoride (Sigma)]. The whole cell lysates were sonicated briefly, and cell debris was removed by centrifugation at 4°C, 13,000rpm for 30 min. Protein concentration of the lysates was determined using bicinchoninic-acid assay (Biorad, Hercules, CA) and 20 μg of proteins were separated using SDS-polyacrylamide (PAGE) gels. Proteins were then transferred on to nitro cellulose (NC) membrane (Millipore, Billerica, MA) and the membranes were incubated with blocking solution (5 % skim milk in 0.1 % Tween 20 and 0.1 % Tris-buffered saline) for 1 hour at room temperature. The membranes were incubated with specific antibodies and then hybridized primary antibodies were

detected using a horseradish peroxidase-conjugated IgG antibody (Santa Cruz Biotechnology). Bands were detected by using the enhanced chemiluminescence kit (Thermo, Rockford, IL, USA).

Animal care and glucose tolerance test

Mice (C57BL/6 male mice, Center for animal resource development, SNU, Seoul, Korea) were fed high fat diet (HFD), consisting of 60 % fat and 6.8 % sucrose (Research diet, New Brunswick, NJ, USA) for 12 weeks. During HFD, DMC (30 mg/kg/day) and Pioglitazone (30 mg/kg/day) dissolved in CrEL (Sigma) was introduced animal by oral gavage for 2 weeks. CrEL has been used as a vehicle for oral gavage. After 2 week treatment, intraperitoneal glucose tolerance test (IP-GTT) was performed. Mice were fasted for 16 hours and then injected with 1g/kg glucose (Sigma) solution. The blood glucose levels were measured at the indicated time points with blood glucose meter (Life scan, Milpitas, CA, USA). All animal studies were approved by the Institutional Animal Care and Use Committee of Seoul National

University Hospital.

Measurement of serum profiles

Mouse serum samples were collected from each group of mice. Blood glucose levels were measured with a blood glucose meter. Serum insulin levels were assessed with an Insulin ELISA kit (Alpco, NH, USA). Plasma TG levels were measured using a triglyceride colorimetric assay kit (Cayman Chemical, MI, USA).

Electron microscopy (TEM)

Mouse gastrocnemius muscle tissue images were evaluated by Transmission Electron Microscopy. In detail, muscle tissues were fixed with 2.5 % Glutaraldehyde in Sodium Cacodylate Buffer (EMS, Hatfield, PA, USA) for 1 h, and then transferred into 5 % glutaraldehyde overnight. After rinsing, tissues were post-fixed with 1% osmium tetroxide for 1 h. Specimens were dehydrated with an ethanol series, and embedded in Araldite-Epon resin (Nissin EM, Tokyo, Japan). Ultrathin sections were stained with uranyl acetate/ lead citrate and photographed with a transmission electron microscope (TEM; JEM-

100CX, JEOL, Tokyo, Japan).

Statistical analysis

Statistical analysis of the data was done with SPSS version 17.0 (SPSS Inc., Chicago, IL). Student's t-test was used to measure the differences between means. Data were expressed as means \pm standard error, and data with *p*-value less than 0.05 are denoted as statistically significant.

<Result>

DMC increases transcriptional activity of PPAR γ

To identify a novel PPAR γ agonist, column chromatography was applied to *Cleistocalyx operculatus* extracts, and 14 compounds were characterized (Figure 1). The 14 compounds were identified and evaluated by transactivation reporter assays with the PPRE tk luciferase assay. Compound 5 showed the most potent activity as a PPAR γ agonist, about 2.5 fold times that of the DMSO control (Figure 2). Compound 5 was identified as DMC (2',4'-dihydroxy-6'-methoxy-3',5'-dimethylchalcone); molecular structure of DMC is shown in (Figure 3). The purity of DMC from *C. operculatus* was confirmed to be over 95 % by HPLC/MS analysis (Figure 4).

To examine whether DMC is able to promote the transcription activity of PPARs, reporter assays were performed. Unexpectedly, DMC also enhanced the transcription activity of PPAR α (Figure 5A), PPAR δ (Figure 5B), and PPAR γ (Figure 5C). Although DMC is able to elevate all isoform of PPARs activity, promoting PPAR γ activity was

most potent among them. Therefore to further confirm the dose-dependent efficacy of the transcriptional activity, DMC and rosiglitazone were treated with various (from low to high) concentrations (Figure 6). To ensure the ligand binding domains (LBDs) of PPAR γ and DMC were combined directly to each other, SPR assay was done (Figure 7). Although DMC was not superior to rosiglitazone, DMC is also a potent PPAR γ ligand.

DMC inhibits adipocyte differentiation of 3T3-L1

Since DMC was found to be a ligand of PPAR γ , I examined whether DMC could stimulate adipogenesis as other PPAR γ agonists do. The adipogenesis of 3T3-L1 preadipocytes was induced by the addition of adipocyte differentiation media (DMI) and the lipid droplets were stained with Oil red O 9 days after the induction of adipogenesis. When rosiglitazone was treated simultaneously with DMI and thereafter, adipocyte differentiation and lipid accumulation were increased compare to the DMSO control. In contrast, DMC treatment inhibited

adipocyte differentiation in a dose-dependent manner, and adipocyte differentiation was completely blocked at a high DMC concentration (20 μ M) (Figure 8A). To determine the stage at which DMC suppressed adipogenesis, DMC was added at several different time points of adipogenesis. Adipocyte differentiation was inhibited when DMC was treated at the very early stage (day 0); however, the inhibitory effect of DMC was not observed when DMC was treated at day 2 or later (Figure 8B). These results suggested that DMC suppressed adipocyte differentiation at the very early stage (within 2 days). Expression pattern of adipogenesis related gene was also examined (Figure 9). DMC efficiently suppressed the expression of C/EBP β and C/EBP δ at the early stages (days 1-2), which resulted in the suppression of their target genes such as PPAR γ and C/EBP α in the next days.

DMC stimulates glucose uptake and fatty acid oxidation in myotubes

I then determined whether DMC could affect glucose uptake

and fatty acid oxidation (FAO), which was known to be affected by PPAR γ activation in myotubes. DMC treatment increased glucose uptake both in the absence and presence of insulin, although the effect was not as great as that of rosiglitazone (Figure 10). In contrast, DMC treatment increased FAO more efficiently than rosiglitazone (Figure 11). Therefore, I also examined the expression of the genes encoding FAO-related proteins. Except for pyruvate dehydrogenase kinase 4 (PDK4), only slight or no increases were observed after DMC treatment in the mRNA levels of FAO-related genes, such as fatty acid translocase (CD36), long-chain acyl-CoA synthetase 1 (ACSL1), carnitine-palmitoyl transferase-1b (CPT1b), and medium-chain acetyl CoA dehydrogenase (MCAD). Rosiglitazone increased the expression of CD36, ACSL1, CPT1b, MCAD, and uncoupling protein 3 (UCP3) (Figure 12). DMC efficiently promoted FAO, but the expressions of PPAR γ -mediated and FAO-related genes such as CD36, ACSL1, and CPT1b were not significantly changed; therefore, another mechanism might be important for FAO stimulation by DMC in addition to PPAR γ

activation.

DMC is potent activator of AMPK

It is well known that AMPK activation ultimately stimulates FAO and glucose uptake in myotubes. I tested whether AMPK activation is involved in FAO stimulation by DMC. When C2C12 myotubes were treated with DMC in the presence of a PPAR γ antagonist, GW9662, or an AMPK inhibitor, compound C, the increase of FAO by DMC was attenuated in the presence of GW9662 and completely abolished in the presence of compound C (Figure 13). To determine whether AMPK can be activated by DMC, AMPK phosphorylation at Thr172 of the α subunit was examined. DMC treatment dramatically increased AMPK phosphorylation, although the phosphorylation levels were lower than those induced by well-known AMPK activators, such as AICAR (Figure 14). Similar to the treatment of AICAR, the induction of AMPK phosphorylation was observed a very short time after the treatment of DMC (within 30 min) (Figure

15A). The phosphorylation of ACC, a downstream substrate of AMPK, which is closely related to AMPK-mediated FAO stimulation, was also examined. Just as AMPK phosphorylation was increased after the DMC treatment, ACC phosphorylation was also increased, indicating that AMPK is activated by DMC. In addition, AMPK phosphorylation was increased by DMC in a dose-dependent manner, and DMC could increase AMPK phosphorylation in lower concentrations than AICAR could (Figure 15B). The DMC-stimulated FAO levels were similar to those of AICAR (Figure. 16). These results indicated that DMC activated AMPK. In general, several AMPK activators promote AMPK phosphorylation by different mechanisms [69]. To determine how DMC activates AMPK activity, following experiments were performed in the present study. To determine whether DMC affected ADP/ATP, cellular ADP and ATP contents were measured (Figure 17). Unlike metformin, DMC did not change ADP/ATP ratio. Therefore, I examined whether DMC directly activates AMPK. DMC induces AMPK activity in a dose-dependent manner in cell free *in vitro* kinase

assay (Figure 18). Furthermore, it was examined here whether DMC activates through directly binding to AMPK complex. In the SPR assay, DMC bound to AMPK, and the affinity of DMC to AMPK was about 3.7 fold higher than that of AMP on the basis of K_d values (Figure 19). These results suggest that DMC is a more effective activator of AMPK. In addition, when both DMC and AICAR was treated to the myocytes, no additive effects was shown in AMPK phosphorylation (Figure 20A), glucose uptake (Figure 20B), and fatty acid oxidation (Figure 20C). When AMP, DMC or mixture of AMP and DMC was injected into AMPK bounded CM5 sensor chip for SPR competition assay, no additive binding was observed (Figure 21), suggesting that they are competitive for a binding site of AMPK.

DMC stimulates fatty acid oxidation in myotubes and inhibits adipogenesis through activating AMPK

To determine whether DMC-induced FAO is mainly mediated by AMPK activation, the expression of AMPK α subunits 1 and 2 was

knocked down by the transfection of specific siRNAs into C2C12 myotubes. The mRNA levels of both AMPK α subunits were dramatically decreased 2 days after the transfection of the siRNAs against the AMPK α 1 and α 2 subunits (siAMPK) (Figure 22A). When the expression of AMPK α subunits were knocked down, the induction of FAO by DMC was no longer observed, indicating that AMPK mediates the DMC-induced FAO increase in C2C12 myotubes (Figure 22B). Reports have shown that AMPK activation suppresses adipocyte differentiation at the early stage of adipogenesis [70, 71]. Therefore, it was also tested here whether AMPK activation was important for the inhibition of adipogenesis by DMC. The 3T3-L1 preadipocytes were transfected with siRNAs against AMPK α subunits the day before the induction of adipocyte differentiation. The expression of AMPK α subunits was efficiently suppressed (Figure 23A), and adipocyte differentiation was not inhibited by DMC in the AMPK-knocked down condition (Figure 23B). The results clearly demonstrated that DMC inhibits adipogenesis by activating AMPK. In conclusion, DMC

treatment regulates fatty acid metabolism in myotubes and adipocyte differentiation mainly through AMPK.

DMC ameliorates high fat diet-induced obesity and glucose tolerance in mice

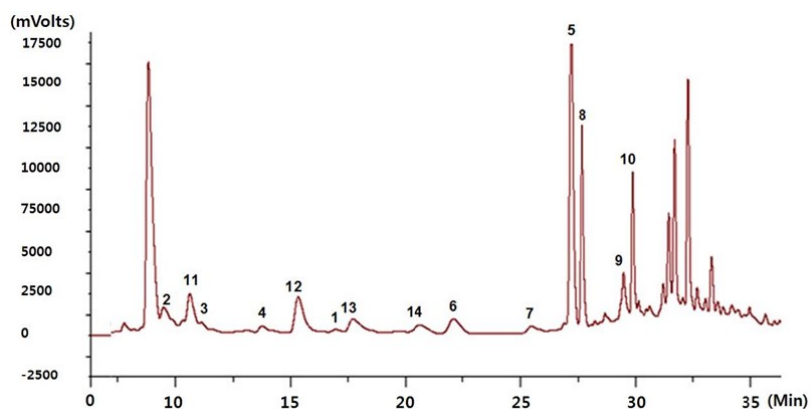
To test whether DMC treatment affects metabolic disorders induced by a high-fat diet (HFD) in mice, mice were fed HFD for 12 weeks and then treated with DMC for 3 weeks. The body weights of the mice treated with DMC were similar to those of the control group 3 weeks after the treatment. (Figure 24). Average food intake (Figure 25A) and water intake (Figure 25B) difference between the groups was insignificant, suggesting that body weight change is not due to food consumption change. I also performed a glucose tolerance test (GTT) using the mice treated with DMC. The glucose tolerance of DMC-treated mice was improved compared with the Veh-treated mice (Figure 26). Next, serum glucose, insulin, and TG level were measured to examine whether DMC improves metabolic abnormalities *in vivo*.

DMC significantly reduced fasting blood glucose level (Figure 27A), normal glucose level (Figure 27B), insulin (Figure 27C) and serum TG (Figure 27D). These data suggest that DMC would improve serum glucose and lipid profiles. The rates of white adipose tissue weight versus total body weight of the DMC-treated mice were lower than those of the control mice (Figure 28). To evaluate adipose tissue histology, epididymal white adipose tissue sections were stained by H&E. The DMC-treated group size of adipocytes was smaller than that of the vehicle group (Figure 29A-B). To identify exact values, more than 10 images of each group were quantified by computerized method (Figure 29C-D). The DMC-treated group's average adipocyte surface area was smaller than that of the Veh-treated group. When array in order to adipocytes size, DMC-treated group is more frequent smaller size than Veh-treated group. To test whether DMC treatment reduces adipose tissue mass through lipolysis or lipogenesis, pRT-PCR was performed with specific primers. DMC significantly increased levels of lipolysis-related genes such as ATGL (Figure 30A), HSL (Figure 30B),

and Perilipin (Figure 30C). Next, DMC significantly reduced lipogenic genes such as ADD1/SREBP1c (Figure 31A), FASN (Figure 31B), and DGAT (Figure 31C). Also I tested adipogenic genes such as C/EBP β (Figure 32A), C/EBP δ (Figure 32B), PPAR γ (Figure 32C), and C/EBP α (Figure 32D). Taken together, these data suggest that DMC efficiently induces lipolysis and reduces lipogenesis and adipogenesis.

Consistent with the results in the cultured muscle cell, AMPK phosphorylation (Figure 33) and fatty acid oxidation rates in the muscles of the DMC-treated mice were substantially higher than those of the Veh-treated mice (Figure 34). When muscle tissue was observed under transmission electron microscope, lipid droplet was decreased in the muscle of the DMC-treated mice compared to that of Veh-treated mice (Figure 35).

These results suggest that DMC probably improves obesity and glucose intolerance by stimulating FAO and inhibiting adipogenesis *in vivo*, which is consistent with the results in the adipocytes.



1	7-Hydroxy-5-methoxy-6,8-dimethylisoflavone	8	2',4'-Dihydroxy-3'-methyl-6'-methoxychalcone
2	5,7-Dihydroxy-6,8-dimethyldihydroflavonol	9	6-Formyl-8-methyl-7-O-methylpinocembrin
3	2,7-Dihydroxy-5-methoxy-6,8-dimethylflavanone	10	(2S)-8-Formyl-5-hydroxy-7-methoxy-6-methylflavanone
4	4,2',4'-Trihydroxy-6'-methoxy-3',5'-dimethylchalcone	11	7-Hydroxy-5-methoxy-8-methylflavanone
5	2',4'-Dihydroxy-6'-methoxy-3',5'-dimethylchalcone	12	8-methylpinocembrin
6	5-hydroxy-7-methoxy-6,8-dimethylflavanone	13	5,7-Dihydroxy-6,8-dimethylflavanone
7	7-Hydroxy-5-methoxy-6,8-dimethylflavanone	14	2,2',4'-Trihydroxy-6'-methoxy-3',5'-dimethylchalcone

The experiment by WK Oh's Lab

Fig 1. Chromatographic figure of *Cleistocalyx operculatus* extracts
 NMR spectra were measured on a Bruker Avance 500 or 600 MHz spectrometer at Seoul National University. HRESIMS were recorded on an Agilent 6530 Q-TOF (Agilent Technologies, Inc., Santa Clara, CA, USA) spectrometer. Silica gel (Merck, 63–200 μm particle size) and RP-18 (Merck, 40–63 μm particle size) were used for column chromatography. TLC was carried out with silica gel 60 F₂₅₄ and RP-18 F₂₅₄ plates. HPLC was carried out using a Gilson system with a UV detector and Optima Pak C₁₈ column (10 \times 250 mm, 10 μm particle size, RS Tech, Korea).

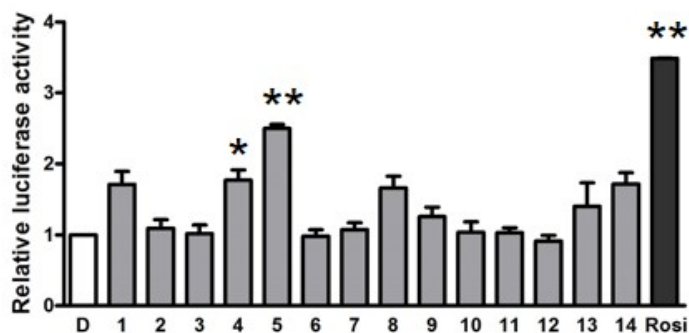
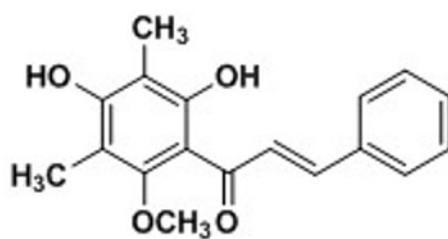


Fig 2. *Cleistocalyx operculatus* extracts enhances transcriptional activity of PPAR γ

Cos7 cells were transiently transfected with PPAR γ expression vector, PPRE-tk luciferase vector and CMV- β -gal for transfection efficiency control. 10 μ M of *Cleistocalyx operculatus* extracts and rosiglitazone (Rosi) were treated for 24 hours. Harvested cells were analyzed by luciferase assay. The number indicates the isolated each molecule of *C. operculatus* extracts via column chromatography (Fig 1). The value of the cells treated with D (DMSO) was set to 1 and the others were expressed as relatives to that. Each bar represents mean \pm S.E. of three independent experiments. * $p < 0.05$ vs. D, ** $p < 0.01$ vs. D

(A)



(B)

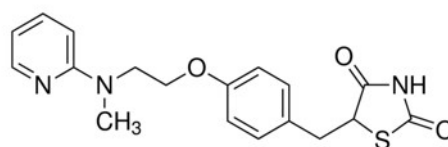
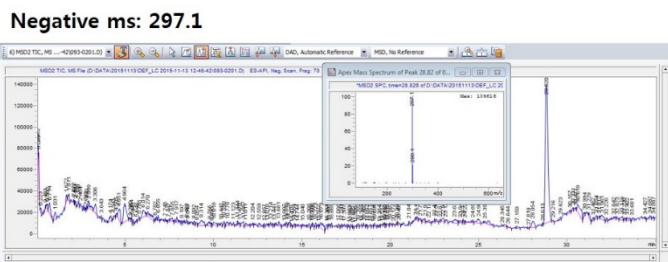
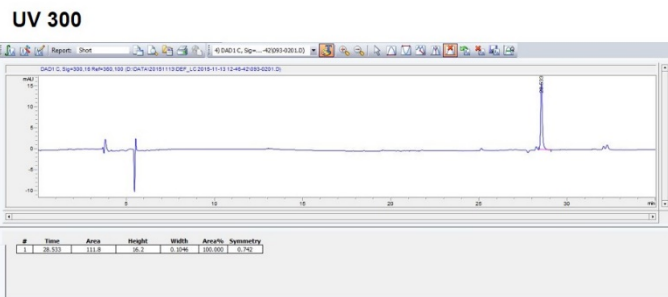
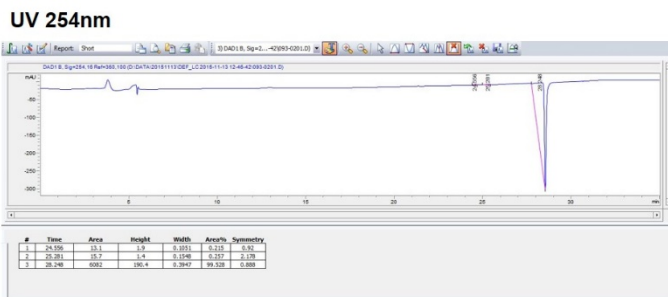


Fig 3. Molecular structure of DMC and rosiglitazone

(A) DMC (2',4'-Dihydroxy-6'-methoxy-3',5'-dimethylchalcone), (B) rosiglitazone.



The experiment by WK Oh's Lab

Fig 4. Purity and quality of DMC isolated from *Cleistocalyx operculatus*

Analysis for purity of DMC was performed on an Agilent Series 1100 LC system (Agilent Technologies, Waldbronn, Germany). The LC system was coupled to an Agilent Series 1100 MSD single quadrupole (Agilent Technologies) equipped with API-ES source. MS detection was conducted in the scan mode. Samples were separated on a reverse-phase column (INNO C18 column, 150 × 4.6 mm I.D., particle size 5 μM, 120 Å) from Young Jin Biochrom (Sungnam, Korea).

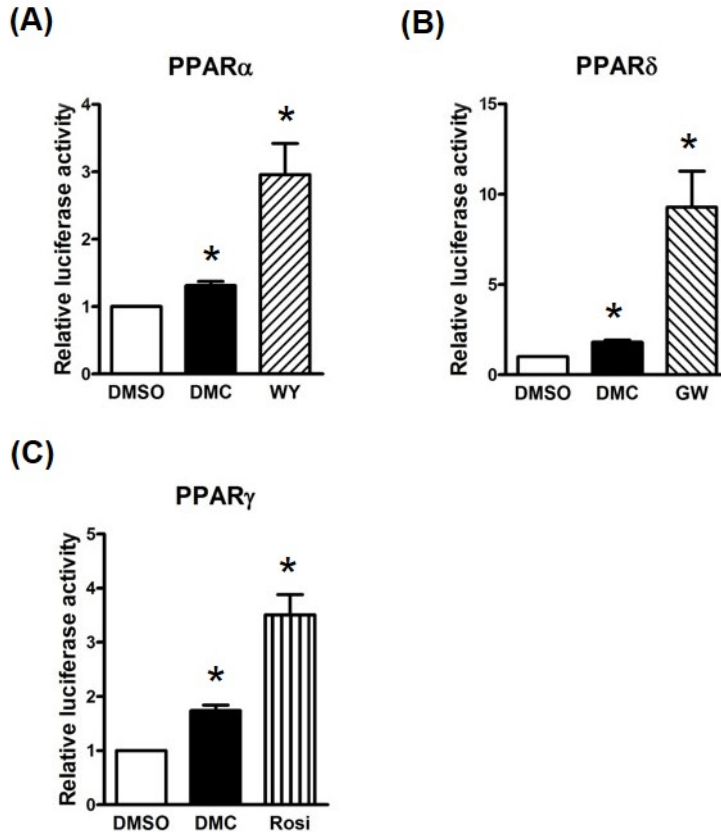


Fig 5. DMC enhances transcriptional activity of PPAR (α , γ and δ)
 Cos7 cells were transiently transfected with PPAR α (A), PPAR δ (B) and PPAR γ (C) expression vector, PPRE-tk luciferase vector and CMV- β -gal for transfection efficiency control. 10 μ M of WY14643 (WY), GW501516 (GW), rosiglitazone (Rosi) was treated for 24 hours. Harvested cells were analyzed by luciferase assay. The value of the cells treated with vehicle was set to 1 and the others were expressed as relatives to that. Each bar represents mean \pm S.E. of three independent experiments. * $p < 0.01$ vs. vehicle

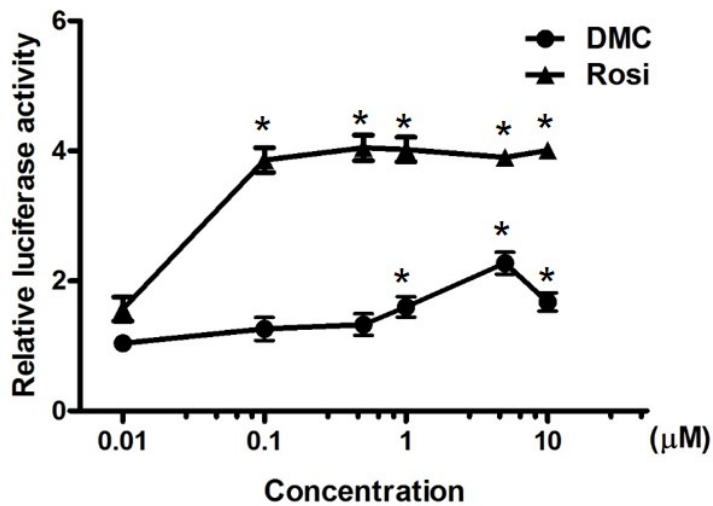
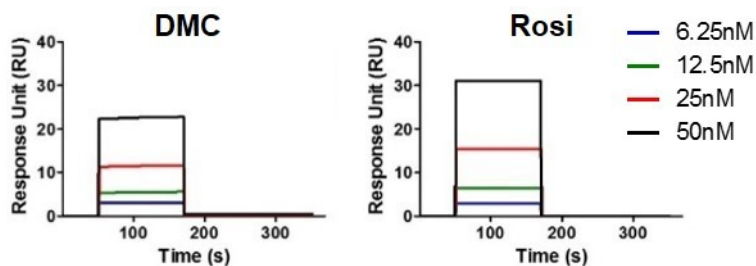


Fig 6. Dose dependent treatment of DMC enhances transcriptional activity of PPAR γ

Cos7 cells were transiently transfected with PPAR γ expression vector, PPRE-tk luciferase vector and cytomegalovirus (CMV)- β -gal for transfection efficiency control. Dose dependent treatment of DMC and rosiglitazone (Rosi) was treated for 24 hours. Harvested cells were analyzed by luciferase assay. The value of the cells treated with DMC 0.01 μ M was set to 1 and the others were expressed as relatives to that. Each bar represents mean \pm S.E. of three independent experiments. * $p < 0.05$ vs. DMC 0.01 μ M



Parameter	Ka (1/Ms)	Kd (1/s)	KD (M)
DMC	4.85×10^3	0.001495	3.28×10^{-7}
Rosi	4.50×10^4	0.001407	3.13×10^{-8}

The experiment by Inhee Mook-Jung's Lab

Fig 7. Physical interaction of DMC with PPAR γ LBD domain

SPR spectroscopy analysis was performed to figure out the binding of DMC and rosiglitazone (Rosi) to PPAR γ LBD. Binding affinity and pharmacokinetic information were determined as described under "Materials and Methods". Data represent the means \pm S.E. of three independent experiments.

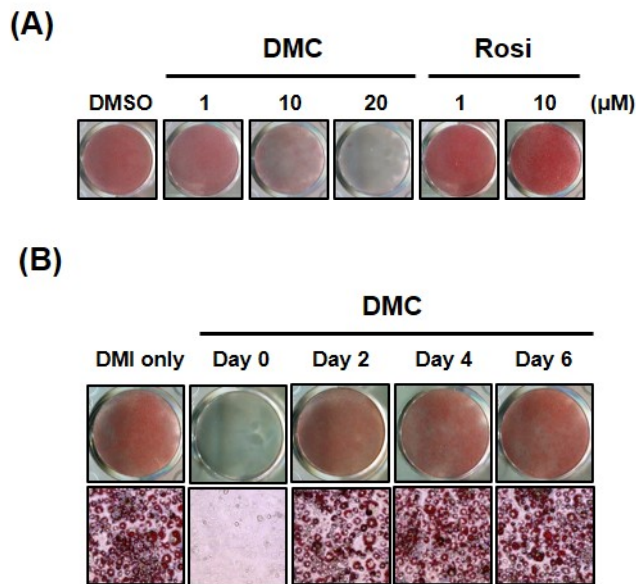


Fig 8. Effect of DMC on 3T3-L1 adipocyte differentiation

(A) DMC or rosiglitazone (Rosi) was treated to 3T3-L1 preadipocytes in the indicated concentrations simultaneously with the induction of adipocyte differentiation (DMI treatment) and continuously thereafter. The cells were stained with Oil red O 9 days after the adipogenesis induction. (B) DMC (20 μM) was treated at the indicated time points during adipogenesis and continuously treated until day 9. Cells were stained with Oil red O at day 9. Lipid droplets were observed using bright field microscopy at 400x magnification (lower panel).

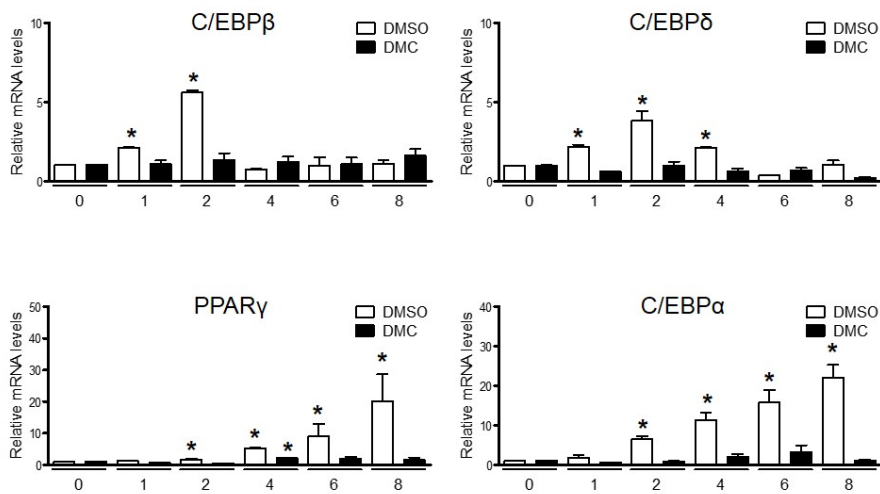


Fig 9. mRNA expression profile of adipogenesis related gene

3T3-L1 preadipocytes were treated with vehicle or DMC (20 μ M) simultaneously with the induction of adipocyte differentiation (DMI treatment). Cells were harvested at indicated day (0, 1, 2, 4, 6 and 8). Total RNAs were isolated and qRT-PCR was performed using specific primers. The mRNA level of each gene obtained from the cells treated with vehicle only at day 0 was set to 1 and the others were expressed as relatives to that. Data represent the mean \pm S.E. of three independent experiments. *, $P < 0.05$ compared with the value of the cells treated with vehicle only at day 0.

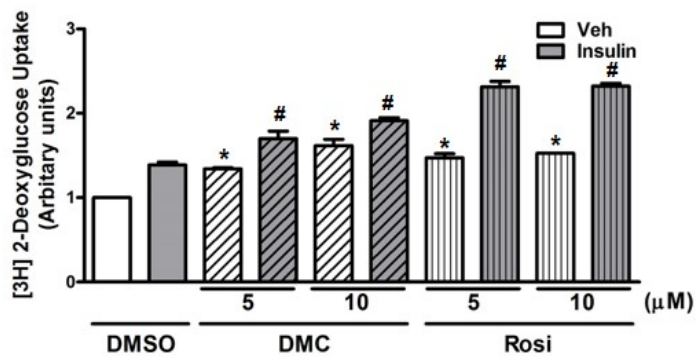


Fig 10. Effect of DMC on glucose uptake in rat skeletal muscle cells

L6 myotubes were treated with DMC (5 μM or 10 μM) or rosiglitazone (Rosi) (5 μM or 10 μM) for 48 h. After insulin treatment for 30 min, glucose uptake was measured. The value of the cells treated with vehicle only in the absence of insulin was set to 1 and the others were expressed as relatives to that. Data represent the means ± S.E. of the three independent experiments. *, $P < 0.05$; compared with the value of the cells treated with vehicle without insulin. #, $P < 0.05$; compared with the value of the cells treated with vehicle with insulin.

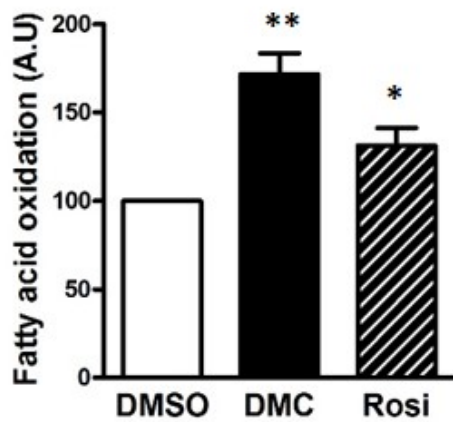


Fig 11. Effect of fatty acid oxidation in mouse skeletal muscle cells
C2C12 myotubes were treated with vehicle, 5 μ M of DMC and 5 μ M of rosiglitazone (Rosi) for 48 h, and then fatty acid oxidation rate was measured. The value of the cells treated with vehicle was set to 100 and the others were expressed as relatives to that. Data represent the means \pm S.E. of five independent experiments. *, $P < 0.05$; **, $P < 0.01$: compared with the value of the cells treated with vehicle.

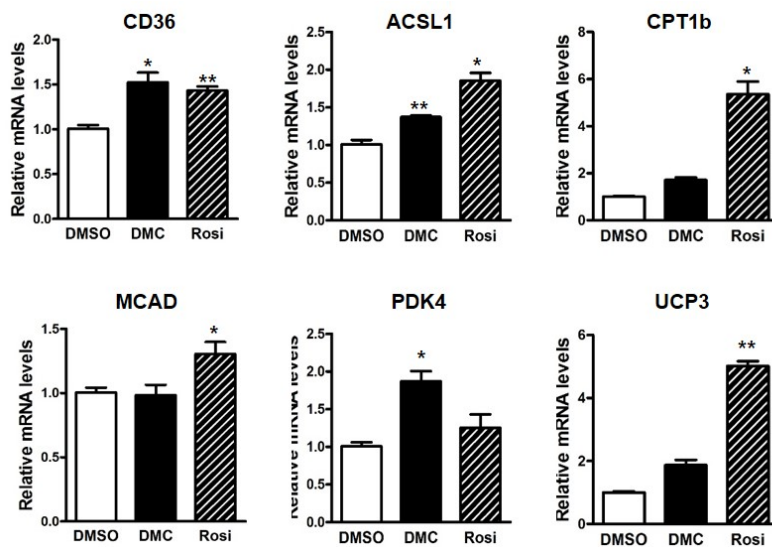


Fig 12. mRNA expression profile of fatty acid oxidation related gene

C2C12 myotubes were treated with vehicle, DMC or rosiglitazone (5 μ M) for 48 h. Total RNAs were isolated and qRT-PCR was performed using specific primers (CD36, ACSL1, CPT1b, MCAD, PDK4, and UCP3). The mRNA level of each gene obtained from the cells treated with vehicle was set to 1 and the others were expressed as relatives to that. Data represent the mean \pm S.E. of three independent experiments. *, $P < 0.05$; **, $P < 0.01$: compared with the value of the cells treated with vehicle.

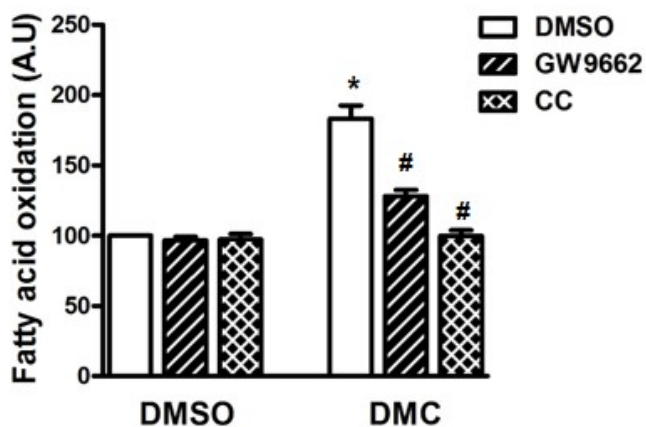


Fig 13. Increased fatty acid oxidation by DMC was abolished with AMPK inhibitor

C2C12 myotubes were pretreated with GW9662 (10 μ M) or compound C (10 μ M) for 1 h and then vehicle, DMC (5 μ M) was added for 48h. The value of the cells treated with vehicle was set to 100 and the others were expressed as relatives to that. Data represent the means \pm S.E. of four independent experiments. *, $P < 0.05$; compared with the value of the cells treated with vehicle. #, $P < 0.05$; compared with the value of the cells treated with DMC only.

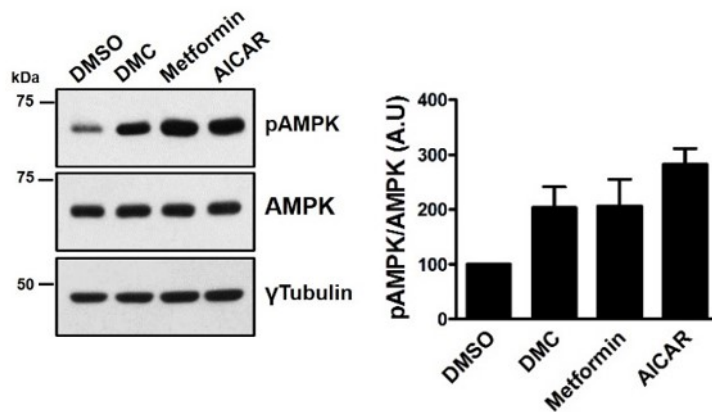


Fig 14. Effect of DMC on AMPK phosphorylation in C2C12 myotubes

C2C12 myotubes were treated vehicle, DMC, metformin (10 mM) and AICAR (1 mM) for 24h. The cell lysates were subjected to western blot analysis with the specific antibodies (left panel). The band intensity of pAMPK was normalized to that of AMPK and the value obtained with the cell lysates from vehicle treated was set to 100 and the others were expressed as relatives to that (right panel). The data represent the means \pm S.E. of four independent experiments. *, $P < 0.05$; compared with the value of the cells treated with vehicle.

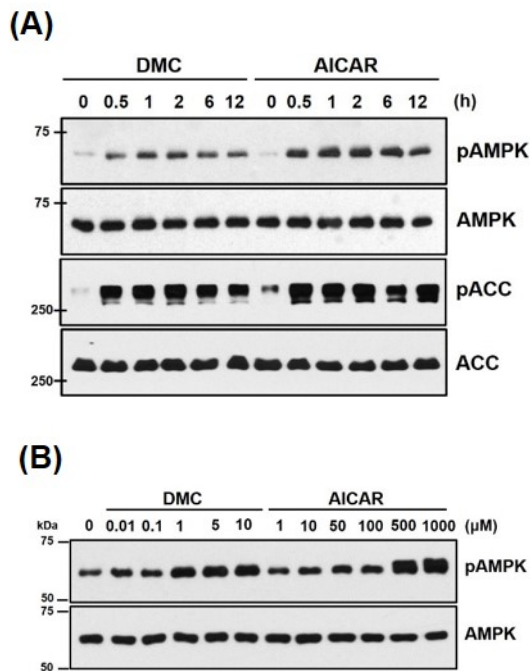


Fig 15. Time and dose dependent effect of DMC on AMPK phosphorylation in C2C12 myotubes

(A) C2C12 myotubes were treated with DMC (5 μ M) or AICAR (1 mM) for the indicated periods, and the lysates were subjected to western blot analysis. (B) C2C12 myotubes were treated with DMC or AICAR in various concentrations for 24 h. The lysates were subjected to western blot analysis.

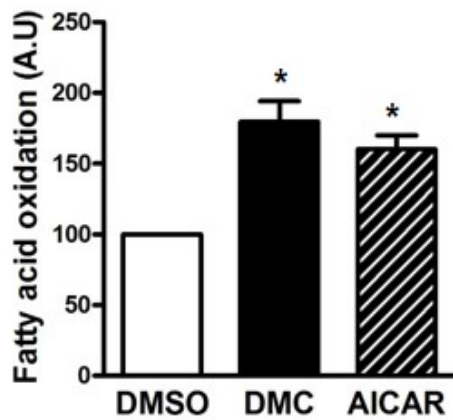


Fig 16. Effect of DMC on fatty acid oxidation in C2C12 myotubes

C2C12 myotubes were treated with vehicle, DMC (5 μ M) and AICAR (1 mM) for 48 h, and then FAO was measured. The value of the cells treated with vehicle was set to 100 and the others were expressed as relatives to that. Data represent the means \pm S.E. of five independent experiments. *, $P < 0.05$; compared with the value of the cells treated with vehicle.

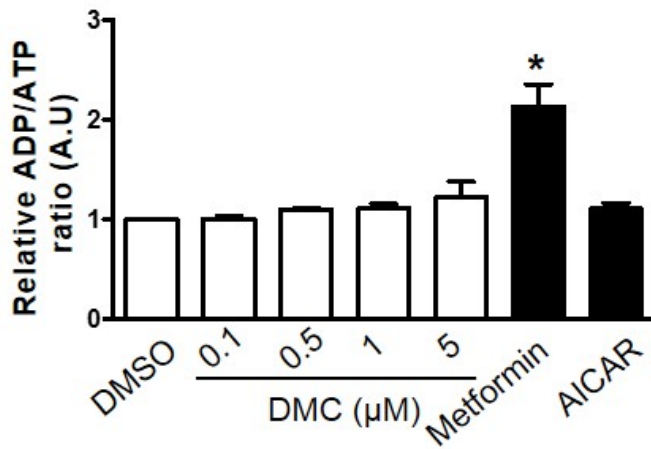


Fig 17. Effect of DMC on ADP/ATP ratio change

C2C12 myotubes were treated with vehicle, different concentration of DMC, metformin (10 mM) and AICAR (1 mM) for 24 h, and then ADP/ATP ratio was measured. The value of the cells treated with vehicle was set to 1 and the others were expressed as relatives to that. Data represent the means \pm S.E. of four independent experiments. *, $P < 0.05$ compared with the value of the cells treated with vehicle.

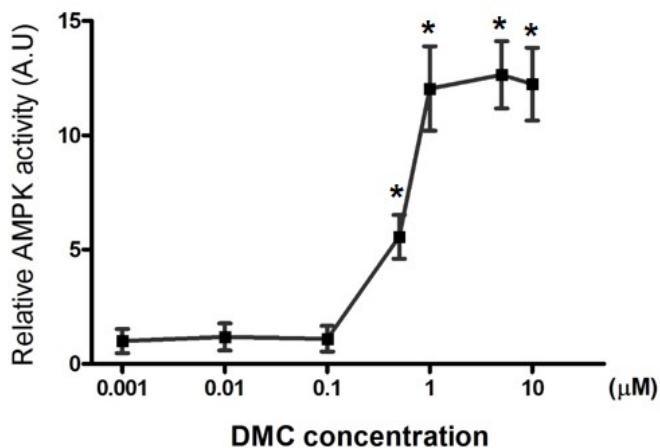
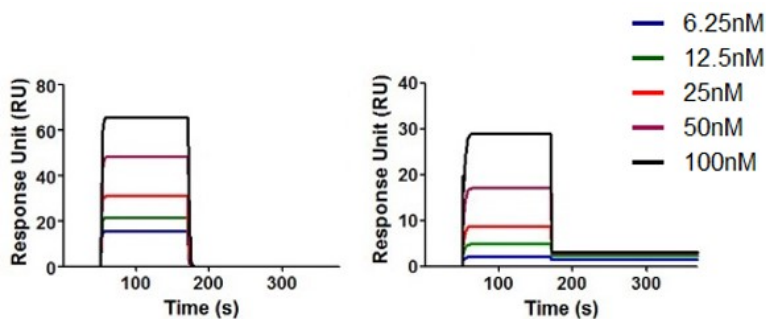


Fig 18. Cell free AMPK activity assay

Cell free *in vitro* kinase assay was performed. Recombinant AMPK complex protein was incubated with different concentration of DMC, then kinase activity was evaluated by phosphorylated synthetic SAMS peptide. The activity obtained with DMC (0.001 μM) treated sample was set to 1. Other values are expressed relative to this value. Data represent the mean \pm S.E. of three independent experiments. * $P < 0.05$ compared with the value of DMC (0.001 μM).



Parameter	Ka (1/Ms)	Kd (1/s)	KD (M)
DMC	3.37×10^{-6}	0.480	1.45×10^{-7}
AMP	1.04×10^{-5}	0.401	3.84×10^{-6}

The experiment by Inhee Mook-Jung's Lab

Fig 19. Physical interaction of DMC with AMPK $\alpha 1\beta 1\gamma 1$

SPR spectroscopy analysis was performed to figure out the binding of DMC and AMP to AMPK complex. Binding affinity and pharmacokinetic information were determined as described under “Materials and Methods”. Data represent the means \pm S.E. of three independent experiments.

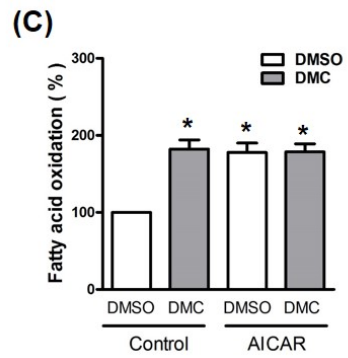
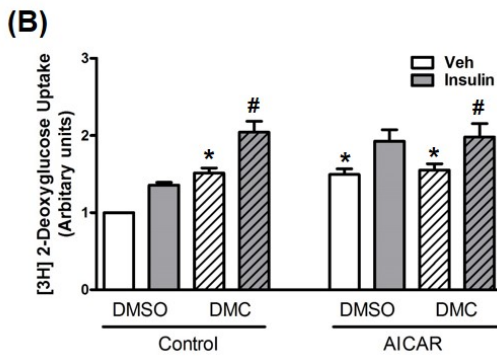
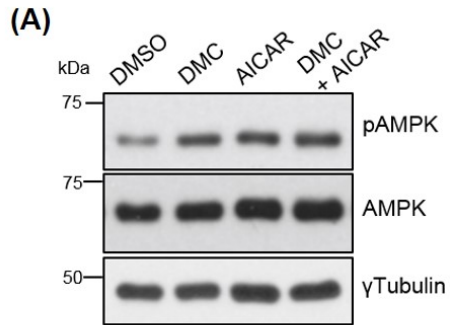
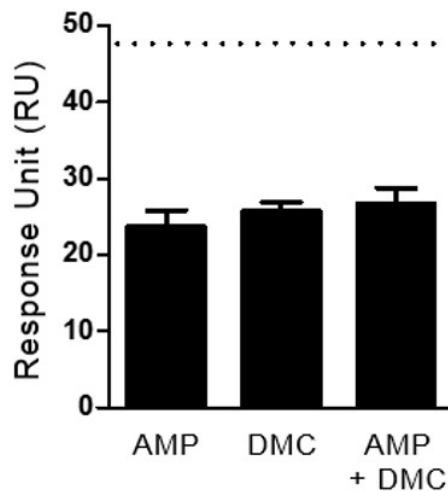


Fig 20. Additive/synergistic effect of DMC and AICAR

(A) C2C12 myotubes were treated with vehicle, DMC (5 μ M), AICAR (1 mM) and mixture of DMC and AICAR for 24 h, and the lysates were subjected to western blot analysis. (B) L6 myotubes were treated with vehicle, DMC, AICAR and mixture of DMC and AICAR for 48 h. After insulin treatment for 30 min, glucose uptake was measured. The value of the cells treated with vehicle only in the absence of insulin was set to 1 and the others were expressed as relatives to that. Data represent the means \pm S.E. of the four independent experiments. *, $P < 0.05$; compared with the value of the cells treated with vehicle without insulin. #, $P < 0.05$; compared with the value of the cells treated with vehicle with insulin. (C) C2C12 myotubes were treated with vehicle, DMC, AICAR and mixture of DMC and AICAR for 48 h, and then FAO was measured. The value of the cells treated with vehicle was set to 100 and the others were expressed as relatives to that. Data represent the means \pm S.E. of four independent experiments. *, $P < 0.05$ compared with the value of the cells treated with vehicle.



Parameter	Response Unit (RU)
AMP	23.78
DMC	25.76
AMP+DMC	26.73

The experiment by Inhee Mook-Jung's Lab

Fig 21. Competition assay of DMC and AICAR to AMPK complex
 SPR spectroscopy analysis was performed to figure out the binding of DMC (100 nM), AMP (100 nM) or mixture DMC and AMP to AMPK. Dotted line represents an expected response unit for noncompetitive binding. Data represent the means \pm S.E. of four independent experiments.

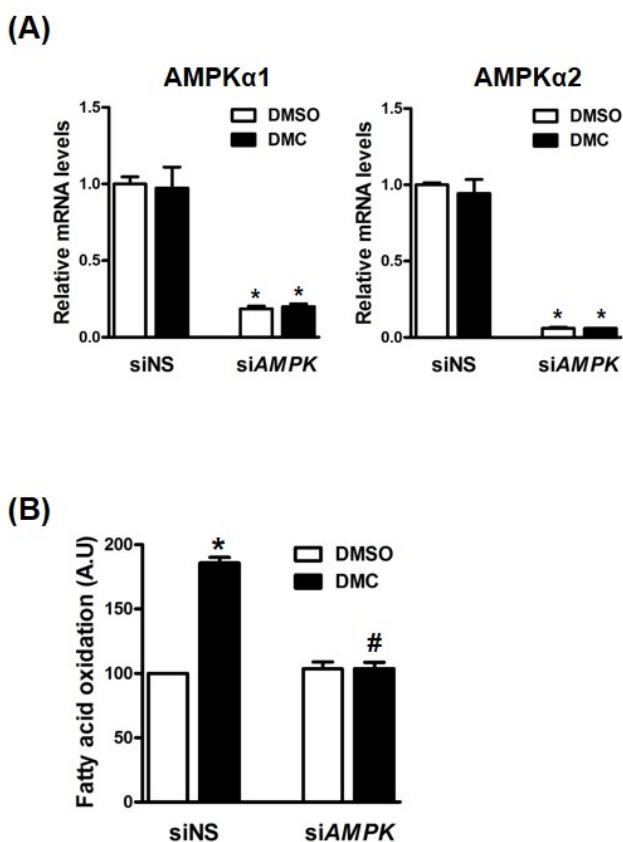


Fig 22. Induction of fatty acid oxidation by DMC is dependent on AMPK

(A and B) C2C12 myotubes were transfected with siRNAs against AMPK α 1 and α 2 subunits (50 nM each, siAMPK) and the next day cells were treated with vehicle or DMC (5 μ M) for 48 h. The mRNA levels of AMPK α 1 and α 2 subunits (A) and FAO (B) were measured. The mRNA level of each gene (A) or FAO (B) value obtained from the cells treated with the control siRNA (siNS) and vehicle was set to 1 or 100, respectively and the others were expressed as relatives to those. Data represent the mean \pm S.E. of three independent experiments. *, $P < 0.05$; compared with the value of the siNS with vehicle. #, $P < 0.05$; compared with the value of the siNS with DMC.

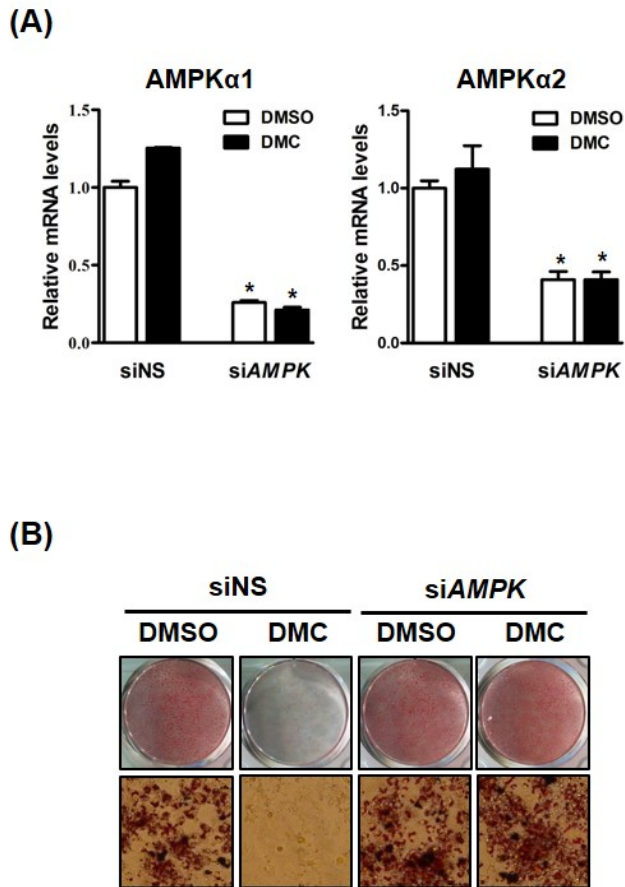


Fig 23. Suppression of adipogenesis is dependent on AMPK

(A and B) 3T3-L1 preadipocytes were transfected with siNS or siAMPK the day before the differentiation induction. (A) The mRNA levels of AMPK α 1 and α 2 subunits were measured two days after the siRNA treatment. The mRNA level of each gene obtained from the cells treated with siNS and vehicle was set to 1 and the others were expressed as relatives to that. Data represent the mean \pm S.E. of three independent experiments. *, $P < 0.05$; compared with the value of the control cells. (B) Cells were stained with Oil red O at day 9 of adipogenesis. Lipid droplets were observed using bright field microscopy at 400x magnification (lower panel).

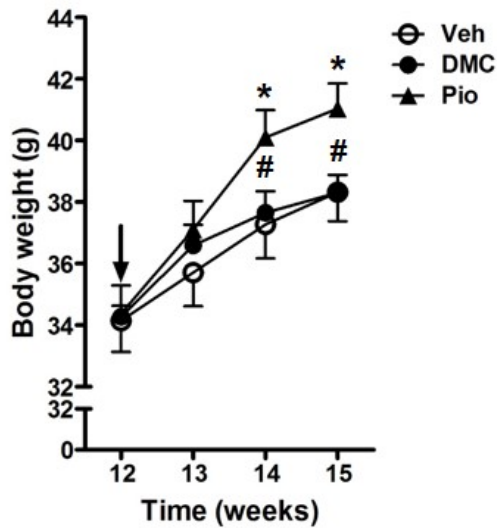


Fig 24. Body weight change in DMC treated diet induced obese mice

Body weights of the mice during the treatments. The arrow indicates the start point of the treatment with DMC or pioglitazone. Each value represents the mean \pm S.E. of each group of mice. *, $P < 0.05$ vs. veh; #, $P < 0.05$ vs. pio at indicated weeks on figure.

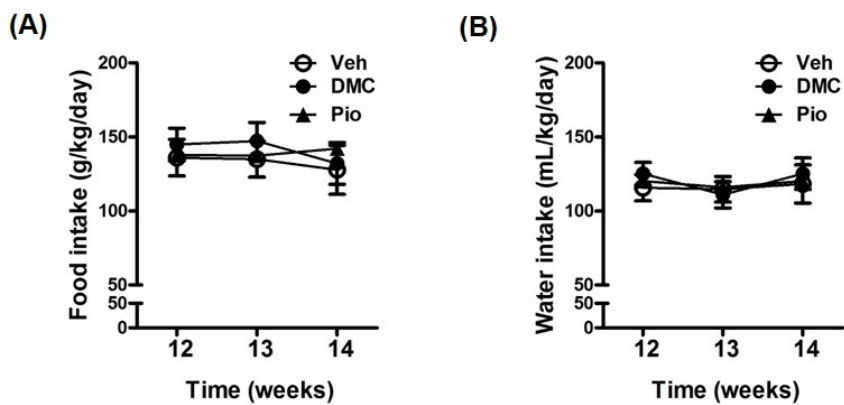


Fig 25. Average daily food and water intake of DMC treated diet induced obese mice

Average daily food and water intake measurement of the mice during the treatments. The measurement was started from 12 weeks to 14 weeks. **(A)** Average daily food intake of each group was shown as line graphs. Data represent the mean \pm S.E. **(B)** Average daily water intake of each group was shown as line graphs. Data represent the mean \pm S.E.

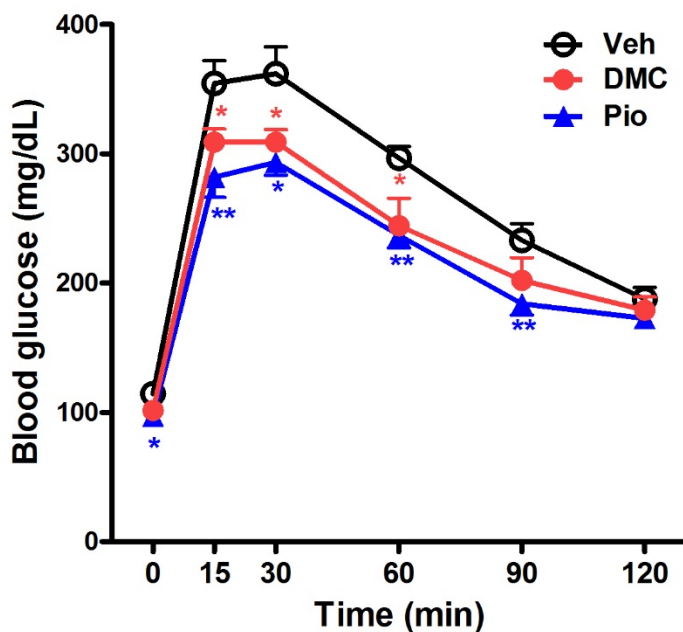


Fig 26. Effect of DMC on glucose tolerance test in diet induced obese mice

DMC-injected mice were fasted for 16 h and injected with glucose solution. Plasma glucose levels were measured from the mouse tail vein blood sample which were drawn at baseline ($t=0$) and indicated time point. Data represent the mean \pm S.E. * $p<0.05$; ** $p<0.01$ vs. veh at indicated time on figure.

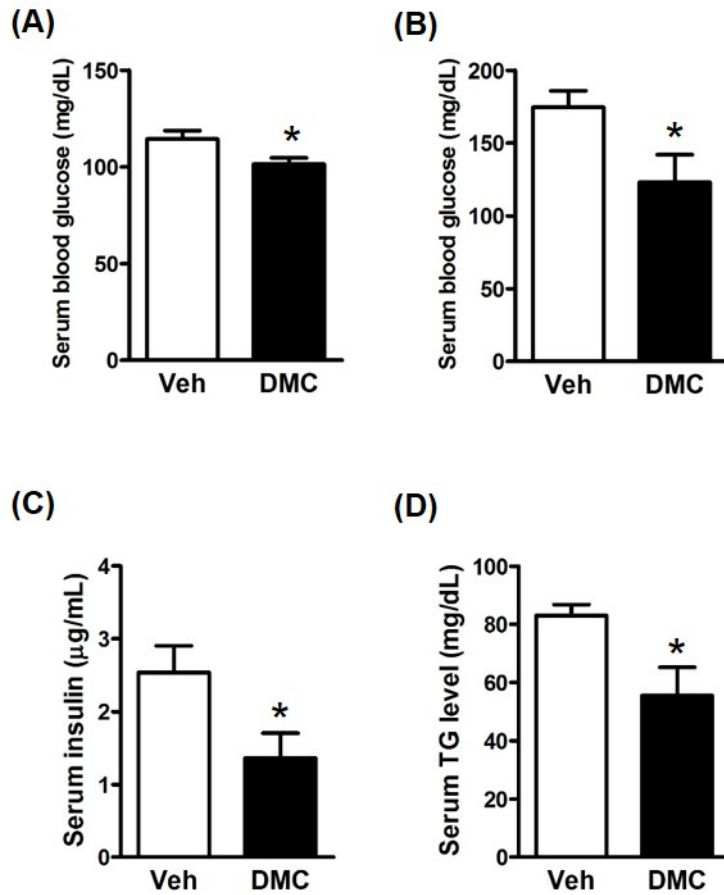


Fig 27. Serum profiles of DMC-treated diet induced obese mice
 Serum concentrations of fasting glucose (A), random glucose (B), insulin (C) and TG (D). Each bar represents the mean \pm S.E. * $p < 0.05$ vs. vehicle compared with the value of the vehicle group.

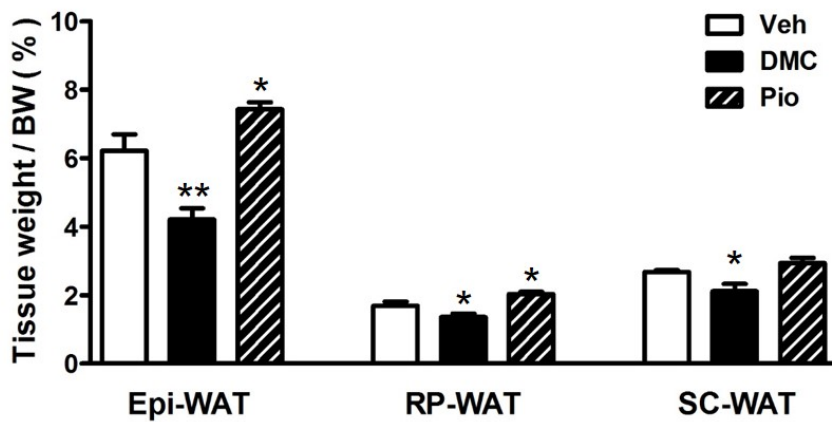


Fig 28. Average tissue weight of DMC treated diet induced obese mice

Each fat tissue weight was measured and then represented as the % value of the total body weight (BW). Each bar represents the mean \pm S.E. * p <0.05 vs. vehicle; ** p <0.01 vs. vehicle at time points indicated on figure.

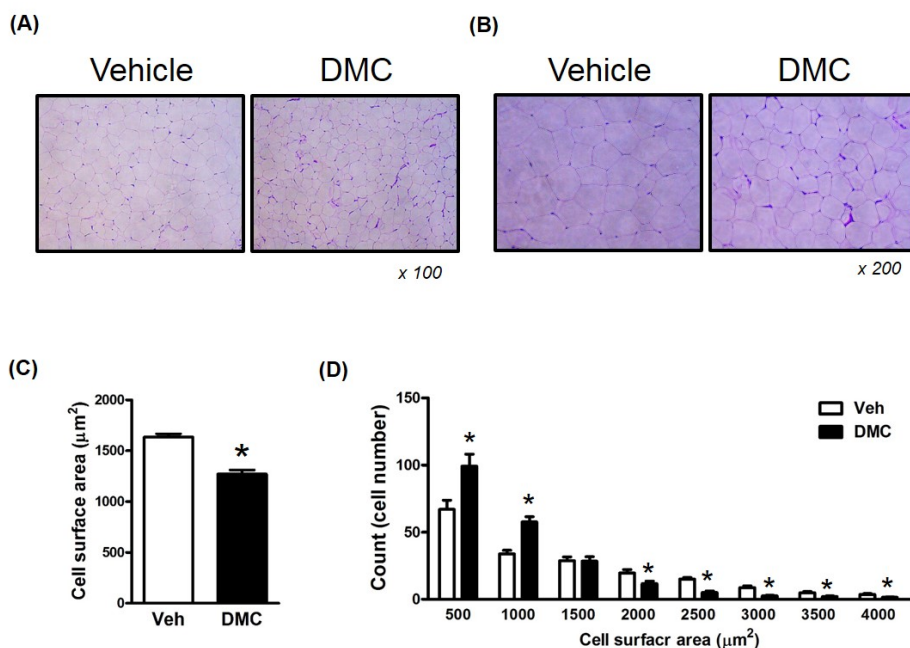


Fig 29. Morphological changes of epididymal white adipose tissue

(A and B) H&E stained epididymal white adipose tissue were observed using bright field microscope. 100x magnification (A) and 200x magnification (B). (C) Adipocytes size were measured and then calculated to cell surface area. Each bar represents the mean \pm S.E. * $p < 0.05$ vs. vehicle compared with the value of the vehicle group. (D) Distribution of cell numbers according to (low to high) adipocyte surface area was measured and then represented as bar graph. * $p < 0.05$; Veh vs. DMC. # $p < 0.05$; Veh vs Pio.

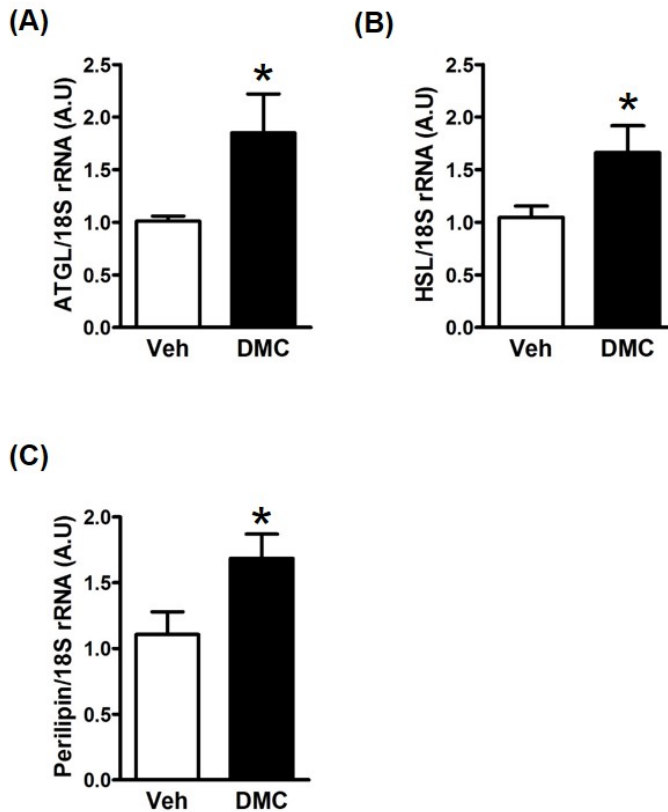


Fig 30. DMC increased lipolysis related genes in epididymal white adipose tissue

Epididymal adipose tissue RNAs were isolated and qRT-PCR was performed using lipolysis related primers adipose triglyceride lipase (ATGL) (A), hormone-sensitive lipase (HSL) (B) and Perilipin (C). The mRNA level of each gene obtained from the mouse adipose tissue treated with veh was set to 1 and the others were expressed as relatives to that. Data represent the mean \pm S.E. of seven individual mice. *, $P < 0.05$ compared with the value of Veh-treated mice.

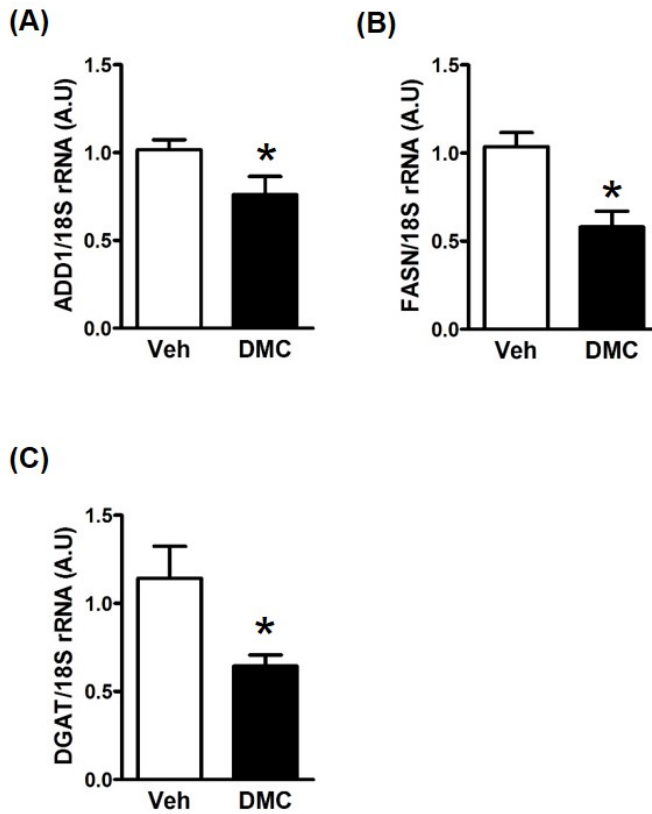


Fig 31. DMC increased lipogenesis related genes in epididymal white adipose tissue

Epididymal adipose tissue RNAs were isolated and qRT-PCR was performed using lipolysis related primers such as adipocyte differentiation and determination factor 1 (ADD1) (A), fatty acid synthase (FASN) (B) and diglyceride acyltransferase (DGAT) (C). The mRNA level of each gene obtained from the mouse adipose tissue treated with veh was set to 1 and the others were expressed as relatives to that. Data represent the mean \pm S.E. of seven individual mice. *, $P < 0.05$ compared with the value of Veh-treated mice.

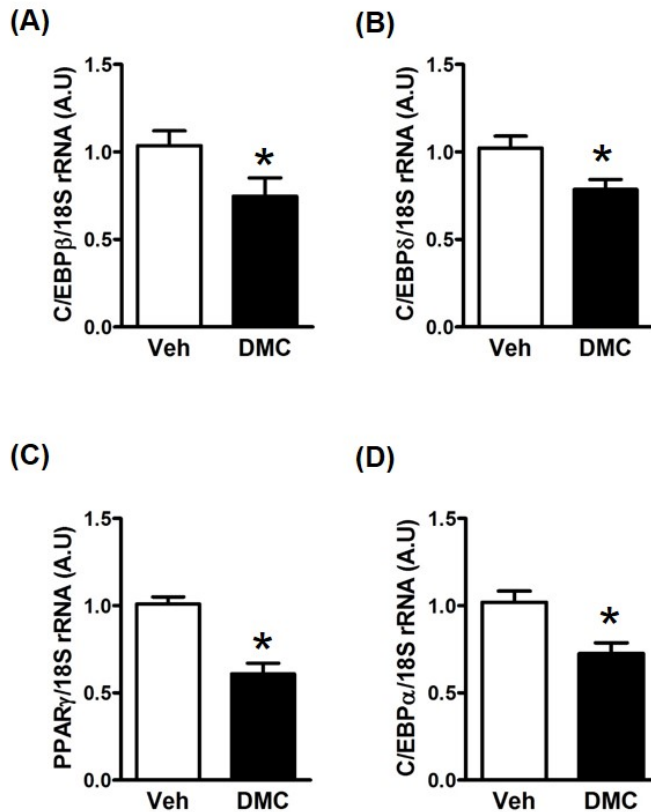
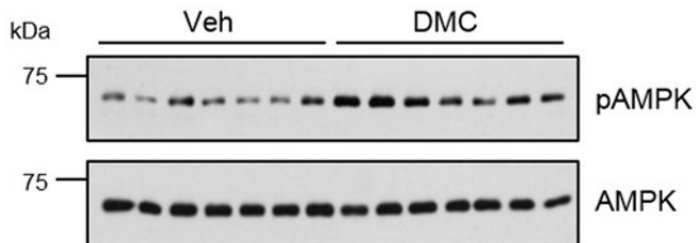


Fig 32. DMC decreased C/EBPs and PPAR γ in epididymal white adipose tissue

Epididymal adipose tissue RNAs were isolated and qRT-PCR was performed using lipolysis related primers C/EBP β (A), C/EBP δ (B), PPAR γ (C) and CEBP α (D). The mRNA level of each gene obtained from the mouse adipose tissue treated with Veh was set to 1 and the others were expressed as relatives to that. Data represent the mean \pm S.E. of seven individual mice. *, $P < 0.05$ compared with the value of Veh-treated mice.

(A)



(B)

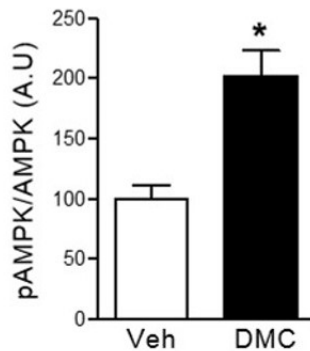


Fig 33. Effect of DMC on AMPK phosphorylation in gastrocnemius muscle

Gastrocnemius muscle tissue was lysed and subjected to western blot analysis with the specific antibodies (A). The band intensity of pAMPK was normalized to that of AMPK and the value obtained with the lysates from Veh-treated mice was set to 100 and the others were expressed as relatives to that (B). The data represent the means \pm S.E. *, $P < 0.05$; compared with the average value of the Veh-treated mice group.

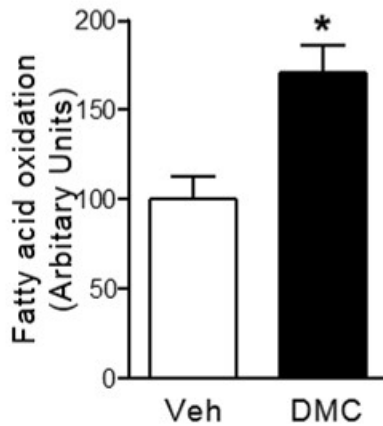


Fig 34. DMC enhances fatty acid oxidation in gastrocnemius muscle

Gastrocnemius muscle tissue was lysed in mitochondria isolation buffer and then fatty acid oxidation (FAO) was measured. The value of the vehicle group was set to 100 and the others were expressed as relatives to that. Data represent the means \pm S.E. of seven individual mice. *, $P < 0.05$ compared with the value of the vehicle group.

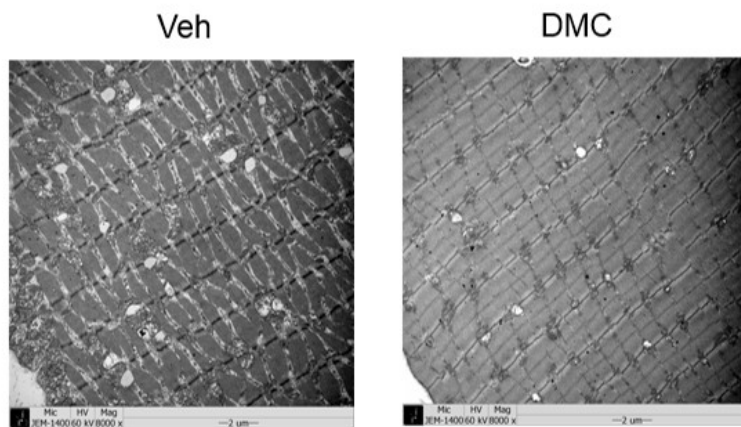


Fig 35. DMC decreased lipid droplet in gastrocnemius muscle tissue

Gastrocnemius muscle tissue were observed using transmission electron microscope (TEM) at 8000x magnification. Electron micrographs of skeletal muscle from vehicle-treated mice (left panel), and DMC-treated mice (right panel).

<Discussion>

Cleistocalyx operculatus is a plant widely distributed in several Southeast Asia countries. Its dried flower bud and leaves have been used as traditional herb tea materials to treat anti-obesity. 2',4'-dihydroxy-6'-methoxy-3',5'-dimethylchalcone (DMC) is a major compound of the *Cleistocalyx operculatus* extract and has been reported to have several health beneficial effects especially regarding metabolic syndrome.

In this study, DMC was isolated from *C. operculatus* extract (Figure 1-4) and elucidated detail mode of action mechanism. First, I screened DMC as a new PPAR γ agonist; however, efficiency in activating PPAR γ was not satisfactory compared to rosiglitazone (Figure 5-7). Although, I found that DMC as a ligand of PPAR γ , however, DMC suppressed adipogenesis (Figure 8-9). Next, I demonstrated that DMC promoted glucose uptake and FAO in myotubes through AMPK phosphorylation (Figure 10-16, 22-23). DMC

promotes AMPK phosphorylation not change ADP/ATP ratio but direct binding to AMPK (Figure 17-19). Furthermore, DMC-treated mice improves insulin tolerance due to high fat diet (Figure 24-35).

AMPK is considered an important therapeutic target for type 2 diabetes, because it is activated under low cellular energy levels and stimulates glucose uptake and fatty acid oxidation, but reduces hepatic glucose production. Numerous pharmacological, natural activators of AMPK have been reported [62]. These activators promote AMPK activity through several different mechanisms [72].

The nucleoside 5-aminoimidazole-4-carboxamide riboside (AICAR) is taken up into cells and is then metabolized to ZMP, which is the AMP analog, by adenosine kinase. ZMP binds to the γ subunit of AMPK and mimics the effect of AMP on allosteric activation of the kinase [73]. Testing of AICAR in an animal model of diabetes exhibited anti-diabetic effects, as many pathological metabolic parameters in these animals, including blood glucose level, lipid profile, hepatic glucose output and glucose disposal, showed improvement [74].

However, AICAR suffers from unfavorable pharmacokinetic properties (i.e., high effective concentration, poor bioavailability and short half-life) and severe metabolic complications such as lactic acidosis and massive uric acid production [75]. In addition, AICAR interacts with S-adenosyl homocysteine hydrolase [76] and glycogen phosphorylase [77], and also inhibits hepatic fructose-1,6-bisphosphatase resulting from accumulation of ZMP [78]. To solve these problems, many researchers have attempted to develop more potent derivatives of AICAR. One example is Example 58 [79], which is structurally related to imidazol analogs of AICAR and increases AMPK activity directly up to 311 % at 200 μ M in comparison with the control treatments.

Guanidine and its isoprenyl derivative, galegine, are natural products from the plant *Galega officinalis*, which was used as a medicinal herb in medieval Europe [80]. Metformin and phenformin are biguanides, synthetic derivatives of guanidine. All of these compounds were tested on animals in the 1920s, but the success of insulin therapy at that time perhaps caused further studies of guanidine-

based drugs to be put on hold. The biguanides were finally introduced for treatment of type 2 diabetes in the 1950s; phenformin was subsequently withdrawn in the 1970s because of a rare but life threatening side effect of lactic acidosis, but metformin is now generally the first choice drug for treatment of type 2 diabetes. Although biguanides were already known to reduce hepatic glucose production and enhance peripheral insulin sensitivity [80], the first clues to their molecular mechanism came in 2000, when it was shown that they inhibited Complex I of the mitochondrial respiratory chain [81, 82]. Interestingly, both drugs are cations, so they accumulate in mitochondria due to the electrical gradient across the inner membrane [81]. Metformin has poor plasma membrane permeability, but uptake into many cells (including hepatocytes) is promoted by the organic cation transporter OCT1, whereas phenformin uptake is less dependent on this transporter [83]. Since both drugs inhibit mitochondrial ATP synthesis, they would be expected to cause increases in the ADP:ATP and AMP:ATP ratios and thus activate AMPK indirectly. AMPK

activation by metformin was indeed demonstrated in 2001 [84], and this was subsequently also shown for phenformin [85] and galegine [86]. The activation mechanism requires increases in AMP and/or ADP, because all three drugs fail to activate AMPK in cells expressing an AMPK γ subunit with a mutation (R531G) that renders the complex AMP/ADP insensitive [83].

In addition to galegine, a bewildering variety of other natural products, many derived from plants used as herbal medicines in Asian countries, have been reported to activate AMPK. These include resveratrol from red grapes, quercetin present in many fruits and vegetables, ginsenoside from *Panax ginseng*, curcumin from *Curcuma longa*, berberine from *Coptis chinensis* (used in the Chinese herbal medicine Huanglian), epigallocatechin gallate from green tea, theaflavin from black tea [87], and hispidulin from snow lotus, another plant used in Chinese herbal medicine [88]. Many of these compounds are claimed to have favorable effects in type 2 diabetes and the metabolic syndrome. Although many of these compounds can be

classed as polyphenols, their structures are quite variable, and a puzzling feature was how such disparate structures would all be able to activate AMPK. Based on findings that berberine inhibited the respiratory chain [89], whereas resveratrol inhibited the F1-ATP synthase [90], it seemed possible that many of them activated AMPK indirectly, by inhibiting mitochondrial ATP production and thus increasing cellular AMP:ATP and/or ADP:ATP ratios, in a similar manner to the biguanides. Supporting this, AMPK activation by resveratrol, berberine, and quercetin was reduced or eliminated in cells expressing the AMP/ADP-insensitive AMPK mutant [83].

Metformin and TZDs indirectly activate AMPK by increasing the AMP:ATP ratio through the inhibition of the mitochondrial respiratory chain complex 1 [72, 91]. In addition, several compounds and natural substances, such as A-769662, PT1, and salicylate, have been reported to activate AMPK by direct binding to AMPK subunits [92-94].

DMC certainly inhibits adipogenesis when it was treated at the beginning step. To consider DMC's anti-adipogenic effect from animal level, adipose tissue were significantly decreased. In general, adipose tissue grows by two mechanisms: hyperplasia (cell number increase) and hypertrophy (cell size increase). Hyperplastic growth appears only at early stages in adipose tissue development. Hypertrophy occurs prior to hyperplasia to meet the need for additional fat storage capacity in the progression of obesity [95-97]. However, it has proven difficult to understand how diet and genetics specifically affect hyperplasia and hypertrophy of adipose cells, because of limited longitudinal data about adipose tissue growth.

Therefore I tried to solve above problem using the indirect method. First, I search for literature about effect of AMPK activators to cell number and cell cycle. There are several reports about AICAR and metformin inhibits proliferation due to S-phase arrest [98-100]. AICAR may regulate cell growth via p53 phosphorylation, and also indicates the possibility of p53 phosphorylation [101]. However, although I did

not observe here, DMC may also regulate cell cycle arrest via the AMPK-p53 pathway. Second, to determine whether DMC has anti-hypertrophy effect, expression level of lipolysis related genes (adipose triglyceride lipase (ATGL), hormone-sensitive lipase (HSL) and Perilipin) and lipogenesis related genes (adipocyte differentiation and determination factor 1 (ADD1), fatty acid synthase (FASN) and diglyceride acyltransferase (DGAT)) was examined here. qRT PCR results shows that DMC interferes with lipid accumulation and consumption via lipolysis and beta-oxidation (Figure 30-32).

However, since DMC is a small molecule and can bind to PPAR γ as well as AMPK, it is possible that DMC also binds to other proteins and modulates their activity. Therefore, AMPK-independent DMC effects should be carefully examined, although any apparent abnormalities were not observed in the mice treated with DMC.

In addition, side effects of animal study with long term treatment using DMC was not verified. In fact, long-term use of metformin has been associated with increased homocysteine levels

[102] and malabsorption of vitamin B12 [103, 104]. Higher doses and prolonged use are associated with increased incidence of vitamin B12 deficiency [105] and some researchers recommend screening or prevention strategies [106].

Further studies such as pharmacokinetics of DMC and effect of mitochondrial activity are needed to elucidate other properties of DMC. Moreover, there was a report that AMPK enhance the mitochondrial biogenesis and functional activity [92]. AMPK enhances the activity of transcription factors like nuclear respiratory factor 1 (NRF-1), myocyte enhancer factor 2 (MEF2), host cell factor (HCF), and others [107, 108]. AMPK also has a positive feedback loop, enhancing its own expression [109].

In this study, DMC, a natural compound, was identified as an activator of AMPK through direct binding. Furthermore, DMC promotes AMPK phosphorylation with a much higher sensitivity than AICAR at much lower concentrations. These data clearly highlighted

DMC as a therapeutic target for the treatment of diabetes, based on the *in vivo* effects of DMC on HFD-induced obese mice.

<Reference>

[1] Dung NT, Kim JM, Kang SC. Chemical composition, antimicrobial and antioxidant activities of the essential oil and the ethanol extract of *Cleistocalyx operculatus* (Roxb.) Merr and Perry buds. *Food and chemical toxicology : an international journal published for the British Industrial Biological Research Association*. 2008;46:3632-9.

[2] Mai TT, Yamaguchi K, Yamanaka M, Lam NT, Otsuka Y, Chuyen NV. Protective and anticataract effects of the aqueous extract of *Cleistocalyx operculatus* flower buds on beta-cells of streptozotocin-diabetic rats. *Journal of agricultural and food chemistry*. 2010;58:4162-8.

[3] Ye CL, Liu JW, Wei DZ, Lu YH, Qian F. In vivo antitumor activity by 2',4'-dihydroxy-6'-methoxy-3',5'-dimethylchalcone in a solid human carcinoma xenograft model. *Cancer chemotherapy and pharmacology*. 2005;55:447-52.

[4] Min BS, Thu CV, Dat NT, Dang NH, Jang HS, Hung TM. Antioxidative flavonoids from *Cleistocalyx operculatus* buds. *Chemical & pharmaceutical bulletin*. 2008;56:1725-8.

[5] Woo AY, Waye MM, Kwan HS, Chan MC, Chau CF, Cheng CH. Inhibition of ATPases by *Cleistocalyx operculatus*. A possible mechanism for the cardiotoxic actions of the herb. *Vascular pharmacology*. 2002;38:163-8.

[6] Min BS, Cuong TD, Lee JS, Shin BS, Woo MH, Hung TM. Cholinesterase inhibitors from *Cleistocalyx operculatus* buds. *Archives of pharmacal research*. 2010;33:1665-70.

[7] Mai TT, Chuyen NV. Anti-hyperglycemic activity of an aqueous extract from flower buds of *Cleistocalyx operculatus* (Roxb.) Merr and Perry. *Bioscience, biotechnology, and biochemistry*. 2007;71:69-76.

- [8] Mai TT, Thu NN, Tien PG, Van Chuyen N. Alpha-glucosidase inhibitory and antioxidant activities of Vietnamese edible plants and their relationships with polyphenol contents. *Journal of nutritional science and vitaminology*. 2007;53:267-76.
- [9] Kim YJ, Ko H, Park JS, Han IH, Amor EC, Lee JW, et al. Dimethyl cardamonin inhibits lipopolysaccharide-induced inflammatory factors through blocking NF-kappaB p65 activation. *International immunopharmacology*. 2010;10:1127-34.
- [10] Ko H, Kim YJ, Amor EC, Lee JW, Kim HC, Kim HJ, et al. Induction of autophagy by dimethyl cardamonin is associated with proliferative arrest in human colorectal carcinoma HCT116 and LOVO cells. *Journal of cellular biochemistry*. 2011;112:2471-9.
- [11] Li DD, Wu XQ, Tang J, Wei XY, Zhu XF. ON-III inhibits erbB-2 tyrosine kinase receptor signal pathway and triggers apoptosis through induction of Bim in breast cancer cells. *Cancer biology & therapy*. 2009;8:739-43.
- [12] Ye CL, Liu JW, Wei DZ, Lu YH, Qian F. In vitro anti-tumor activity of 2',4'-dihydroxy-6'-methoxy-3',5'-dimethylchalcone against six established human cancer cell lines. *Pharmacological research : the official journal of the Italian Pharmacological Society*. 2004;50:505-10.
- [13] Ye CL, Liu JW, Wei DZ, Lu YH, Qian F. In vivo antitumor activity by 2',4'-dihydroxy-6'-methoxy-3',5'-dimethylchalcone in a solid human carcinoma xenograft model. *Cancer chemotherapy and pharmacology*. 2005;56:70-4.
- [14] Ye CL, Liu Y, Wei DZ. Antioxidant and anticancer activity of 3'-formyl-4', 6'-dihydroxy-2'-methoxy-5'-methylchalcone and (2S)-8-formyl-5-hydroxy-7-methoxy-6-methylflavanone. *The Journal of pharmacy and pharmacology*. 2007;59:553-9.
- [15] Ye CL, Qian F, Wei DZ, Lu YH, Liu JW. Induction of apoptosis in K562 human leukemia cells by 2',4'-dihydroxy-6'-methoxy-3',5'-dimethylchalcone. *Leukemia research*. 2005;29:887-92.

- [16] Zhu XF, Xie BF, Zhou JM, Feng GK, Liu ZC, Wei XY, et al. Blockade of vascular endothelial growth factor receptor signal pathway and antitumor activity of ON-III (2',4'-dihydroxy-6'-methoxy-3',5'-dimethylchalcone), a component from Chinese herbal medicine. *Molecular pharmacology*. 2005;67:1444-50.
- [17] Huang HY, Niu JL, Lu YH. Multidrug resistance reversal effect of DMC derived from buds of *Cleistocalyx operculatus* in human hepatocellular tumor xenograft model. *Journal of the science of food and agriculture*. 2012;92:135-40.
- [18] Huang HY, Niu JL, Zhao LM, Lu YH. Reversal effect of 2',4'-dihydroxy-6'-methoxy-3',5'-dimethylchalcone on multi-drug resistance in resistant human hepatocellular carcinoma cell line BEL-7402/5-FU. *Phytomedicine : international journal of phytotherapy and phytopharmacology*. 2011;18:1086-92.
- [19] Qian F, Ye CL, Wei DZ, Lu YH, Yang SL. In vitro and in vivo reversal of cancer cell multidrug resistance by 2',4'-dihydroxy-6'-methoxy-3',5'-dimethylchalcone. *Journal of chemotherapy (Florence, Italy)*. 2005;17:309-14.
- [20] Martinez A, Conde E, Moure A, Dominguez H, Estevez RJ. Protective effect against oxygen reactive species and skin fibroblast stimulation of *Couroupita guianensis* leaf extracts. *Natural product research*. 2012;26:314-22.
- [21] Skandrani I, Limem I, Neffati A, Boubaker J, Ben Sghaier M, Bhourri W, et al. Assessment of phenolic content, free-radical-scavenging capacity genotoxic and anti-genotoxic effect of aqueous extract prepared from *Moricandia arvensis* leaves. *Food and chemical toxicology : an international journal published for the British Industrial Biological Research Association*. 2010;48:710-5.
- [22] Su MY, Huang HY, Li L, Lu YH. Protective effects of 2',4'-dihydroxy-6'-methoxy-3',5'-dimethylchalcone to PC12 cells against cytotoxicity induced by hydrogen peroxide. *Journal of agricultural and food chemistry*. 2011;59:521-7.

- [23] Yu WG, Qian J, Lu YH. Hepatoprotective effects of 2',4'-dihydroxy-6'-methoxy-3',5'-dimethylchalcone on CCl₄-induced acute liver injury in mice. *Journal of agricultural and food chemistry*. 2011;59:12821-9.
- [24] Amor EC, Villasenor IM, Ghayur MN, Gilani AH, Choudhary MI. Spasmolytic flavonoids from *Syzygium samarangense* (Blume) Merr. & L.M. Perry. *Zeitschrift fur Naturforschung C, Journal of biosciences*. 2005;60:67-71.
- [25] Ghayur MN, Gilani AH, Khan A, Amor EC, Villasenor IM, Choudhary MI. Presence of calcium antagonist activity explains the use of *Syzygium samarangense* in diarrhoea. *Phytotherapy research : PTR*. 2006;20:49-52.
- [26] Gafner S, Wolfender JL, Mavi S, Hostettmann K. Antifungal and antibacterial chalcones from *Myrica serrata*. *Planta medica*. 1996;62:67-9.
- [27] Salem MM, Werbovetz KA. Antiprotozoal compounds from *Psoralea argyrea*. *Journal of natural products*. 2005;68:108-11.
- [28] Dao TT, Tung BT, Nguyen PH, Thuong PT, Yoo SS, Kim EH, et al. C-Methylated Flavonoids from *Cleistocalyx operculatus* and Their Inhibitory Effects on Novel Influenza A (H1N1) Neuraminidase. *Journal of natural products*. 2010;73:1636-42.
- [29] Hu YC, Hao DM, Zhou LX, Zhang Z, Huang N, Hoptroff M, et al. 2',4'-Dihydroxy-6'-methoxy-3',5'-dimethylchalcone protects the impaired insulin secretion induced by glucotoxicity in pancreatic beta-cells. *Journal of agricultural and food chemistry*. 2014;62:1602-8.
- [30] Luo Y, Lu Y. 2', 4'-dihydroxy-6'-methoxy-3', 5'-dimethylchalcone inhibits apoptosis of MIN6 cells via improving mitochondrial function. *Die Pharmazie-An International Journal of Pharmaceutical Sciences*. 2012;67:798-803.
- [31] Jin X, Wei X, Huang Z, Wu D. Identify and Characterize the PPAR- γ Ligand-

binding Activity of Extracts of *Cleistocalyx operculatus*. *J Anhui Agric Sci*. 2008;36:9106-9.

[32] James W. The fundamental drivers of the obesity epidemic. *Obesity Reviews*. 2008;9:6-13.

[33] Bleich S, Cutler D, Murray C, Adams A. Why is the developed world obese? : National Bureau of Economic Research; 2007.

[34] Kopelman PG. Obesity as a medical problem. *Nature*. 2000;404:635-43.

[35] Willett WC, Dietz WH, Colditz GA. Guidelines for healthy weight. *New England Journal of Medicine*. 1999;341:427-34.

[36] Ritz E, Rychlík I, Locatelli F, Halimi S. End-stage renal failure in type 2 diabetes: A medical catastrophe of worldwide dimensions. *American journal of kidney diseases*. 1999;34:795-808.

[37] Creager MA, Lüscher TF, Cosentino F, Beckman JA. Diabetes and vascular disease pathophysiology, clinical consequences, and medical therapy: part I. *Circulation*. 2003;108:1527-32.

[38] Wang F, Javitt JC. Eye care for elderly Americans with diabetes mellitus: failure to meet current guidelines. *Ophthalmology*. 1996;103:1744-50.

[39] Young M, Boulton A, MacLeod A, Williams D, Sonksen P. A multicentre study of the prevalence of diabetic peripheral neuropathy in the United Kingdom hospital clinic population. *Diabetologia*. 1993;36:150-4.

[40] Hamby RI, Zoneraich S, Sherman L. Diabetic cardiomyopathy. *Jama*. 1974;229:1749-54.

[41] Chang A, Wyse B, Gilchrist B, Peterson T, Diani A. Ciglitazone, a New

Hypoglycemic Agent: I. Studies in ob/ob and db/db Mice, Diabetic Chinese Hamsters, and Normal and Streptozotocin-Diabetic Rats. *Diabetes*. 1983;32:830-8.

[42] Chang AY, Wyse BM, Gilchrist BJ. Ciglitazone, a New Hypoglycemic Agent: II. Effect on Glucose and Lipid Metabolisms and Insulin Binding in the Adipose Tissue of C57BL/6J-ob/ob and +/? Mice. *Diabetes*. 1983;32:839-45.

[43] Fujita T, Sugiyama Y, Taketomi S, Sohda T, Kawamatsu Y, Iwatsuka H, et al. Reduction of insulin resistance in obese and/or diabetic animals by 5-[4-(1-methylcyclohexylmethoxy) benzyl]-thiazolidine-2, 4-dione (ADD-3878, U-63,287, ciglitazone), a new antidiabetic agent. *Diabetes*. 1983;32:804-10.

[44] Guan HP, Li Y, Jensen MV, Newgard CB, Stepan CM, Lazar MA. A futile metabolic cycle activated in adipocytes by antidiabetic agents. *Nature medicine*. 2002;8:1122-8.

[45] Delea TE, Edelsberg JS, Hagiwara M, Oster G, Phillips LS. Use of thiazolidinediones and risk of heart failure in people with type 2 diabetes a retrospective cohort study. *Diabetes care*. 2003;26:2983-9.

[46] Lu C-J, Sun Y, Muo C-H, Chen R-C, Chen P-C, Hsu CY. Risk of stroke with thiazolidinediones: a ten-year nationwide population-based cohort study. *Cerebrovascular diseases (Basel, Switzerland)*. 2012;36:145-51.

[47] Lenhard MJ, Funk WB. Failure to develop hepatic injury from rosiglitazone in a patient with a history of troglitazone-induced hepatitis. *Diabetes Care*. 2001;24:168-9.

[48] Staels B. Fluid retention mediated by renal PPAR γ . *Cell metabolism*. 2005;2:77-8.

[49] Niemeyer NV, Janney LM. Thiazolidinedione-Induced Edema. *Pharmacotherapy: The Journal of Human Pharmacology and Drug Therapy*. 2002;22:924-9.

- [50] Kliewer SA, Xu HE, Lambert MH, Willson TM. Peroxisome proliferator-activated receptors: from genes to physiology. *Recent progress in hormone research*. 2000;56:239-63.
- [51] Cock Ta HS, Auwerx J. Peroxisome proliferator-activated receptor-gamma: too much of a good thing causes harm. *EMBO Rep*. 2004;5:142-7.
- [52] Levin D, Bell S, Sund R, Hartikainen SA, Tuomilehto J, Pukkala E, et al. Pioglitazone and bladder cancer risk: a multipopulation pooled, cumulative exposure analysis. *Diabetologia*. 2015;58:493-504.
- [53] Chen X, Yang L, Zhai SD. Risk of cardiovascular disease and all-cause mortality among diabetic patients prescribed rosiglitazone or pioglitazone: a meta-analysis of retrospective cohort studies. *Chinese medical journal*. 2012;125:4301-6.
- [54] Baena-González E, Rolland F, Thevelein JM, Sheen J. A central integrator of transcription networks in plant stress and energy signalling. *Nature*. 2007;448:938-42.
- [55] Bokko PB, Francione L, Bandala-Sanchez E, Ahmed AU, Annesley SJ, Huang X, et al. Diverse cytopathologies in mitochondrial disease are caused by AMP-activated protein kinase signaling. *Molecular biology of the cell*. 2007;18:1874-86.
- [56] Gurumurthy S, Xie SZ, Alagesan B, Kim J, Yusuf RZ, Saez B, et al. The Lkb1 metabolic sensor maintains haematopoietic stem cell survival. *Nature*. 2010;468:659-63.
- [57] Hedbacker K, Carlson M. SNF1/AMPK pathways in yeast. *Frontiers in bioscience: a journal and virtual library*. 2008;13:2408.
- [58] Johnson EC, Kazgan N, Bretz CA, Forsberg LJ, Hector CE, Worthen RJ, et al. Altered metabolism and persistent starvation behaviors caused by reduced AMPK function in *Drosophila*. *PLoS One*. 2010;5:e12799.

- [59] Thelander M, Olsson T, Ronne H. Snf1-related protein kinase 1 is needed for growth in a normal day–night light cycle. *The EMBO journal*. 2004;23:1900-10.
- [60] Apfeld J, O'Connor G, McDonagh T, DiStefano PS, Curtis R. The AMP-activated protein kinase AAK-2 links energy levels and insulin-like signals to lifespan in *C. elegans*. *Genes & development*. 2004;18:3004-9.
- [61] Greer EL, Brunet A. Different dietary restriction regimens extend lifespan by both independent and overlapping genetic pathways in *C. elegans*. *Aging cell*. 2009;8:113-27.
- [62] Hardie DG, Ross FA, Hawley SA. AMPK: a nutrient and energy sensor that maintains energy homeostasis. *Nature reviews Molecular cell biology*. 2012;13:251-62.
- [63] Hardie DG. Minireview: the AMP-activated protein kinase cascade: the key sensor of cellular energy status. *Endocrinology*. 2003;144:5179-83.
- [64] Xiao B, Sanders MJ, Underwood E, Heath R, Mayer FV, Carmena D, et al. Structure of mammalian AMPK and its regulation by ADP. *Nature*. 2011;472:230-3.
- [65] Oakhill JS, Steel R, Chen Z-P, Scott JW, Ling N, Tam S, et al. AMPK is a direct adenylate charge-regulated protein kinase. *Science*. 2011;332:1433-5.
- [66] Hardie DG. AMPK: a target for drugs and natural products with effects on both diabetes and cancer. *Diabetes*. 2013;62:2164-72.
- [67] Merrill GF, Kurth EJ, Hardie DG, Winder WW. AICA riboside increases AMP-activated protein kinase, fatty acid oxidation, and glucose uptake in rat muscle. *The American journal of physiology*. 1997;273:E1107-12.
- [68] McGarry JD. Banting lecture 2001 Dysregulation of fatty acid metabolism in the etiology of type 2 diabetes. *Diabetes*. 2002;51:7-18.

- [69] Dzamko NL, Steinberg GR. AMPK-dependent hormonal regulation of whole-body energy metabolism. *Acta physiologica*. 2009;196:115-27.
- [70] Habinowski SA, Witters LA. The effects of AICAR on adipocyte differentiation of 3T3-L1 cells. *Biochem Biophys Res Commun*. 2001;286:852-6.
- [71] Zhou Y, Wang D, Zhu Q, Gao X, Yang S, Xu A, et al. Inhibitory effects of A-769662, a novel activator of AMP-activated protein kinase, on 3T3-L1 adipogenesis. *Biol Pharm Bull*. 2009;32:993-8.
- [72] Lee WJ, Kim M, Park H-S, Kim HS, Jeon MJ, Oh KS, et al. AMPK activation increases fatty acid oxidation in skeletal muscle by activating PPAR α and PGC-1. *Biochemical and biophysical research communications*. 2006;340:291-5.
- [73] Merrill G, Kurth E, Hardie D, Winder W. AICA riboside increases AMP-activated protein kinase, fatty acid oxidation, and glucose uptake in rat muscle. *American Journal of Physiology-Endocrinology And Metabolism*. 1997;273:E1107-E12.
- [74] Bergeron R, Russell RR, Young LH, Ren J-M, Marcucci M, Lee A, et al. Effect of AMPK activation on muscle glucose metabolism in conscious rats. *American Journal of Physiology-Endocrinology And Metabolism*. 1999;276:E938-E44.
- [75] Goodyear LJ. The exercise pill—too good to be true? *New England Journal of Medicine*. 2008;359:1842-4.
- [76] Fabianowska-Majewska K, Duley JA, Simmonds HA. Effects of novel anti-viral adenosine analogues on the activity of S-adenosylhomocysteine hydrolase from human liver. *Biochemical pharmacology*. 1994;48:897-903.
- [77] Longnus SL, Wambolt RB, Parsons HL, Brownsey RW, Allard MF. 5-Aminoimidazole-4-carboxamide 1- β -d-ribofuranoside (AICAR) stimulates

myocardial glycogenolysis by allosteric mechanisms. *American Journal of Physiology-Regulatory, Integrative and Comparative Physiology*. 2003;284:R936-R44.

[78] Vincent MF, Marangos PJ, Gruber HE, Van den Berghe G. Inhibition by AICA riboside of gluconeogenesis in isolated rat hepatocytes. *Diabetes*. 1991;40:1259-66.

[79] Moinet G, Marais D, Hallakou-Bozec S, Charon C. Use of AMPK-activating imidazole derivatives, preparation process therefor and pharmaceutical compositions comprising them. *Google Patents*; 2012.

[80] Bailey C, Campbell IW, Chan JC, Davidson JA, Howlett H, Ritz P. *Metformin-The gold standard: a scientific handbook*. 2007.

[81] Owen M, DORAN E, Halestrap A. Evidence that metformin exerts its anti-diabetic effects through inhibition of complex I of the mitochondrial respiratory chain. *Biochem J*. 2000;348:607-14.

[82] El-Mir M-Y, Nogueira V, Fontaine E, Avéret N, Rigoulet M, Leverve X. Dimethylbiguanide inhibits cell respiration via an indirect effect targeted on the respiratory chain complex I. *Journal of Biological Chemistry*. 2000;275:223-8.

[83] Hawley SA, Ross FA, Chevtzoff C, Green KA, Evans A, Fogarty S, et al. Use of cells expressing γ subunit variants to identify diverse mechanisms of AMPK activation. *Cell metabolism*. 2010;11:554-65.

[84] Zhou G, Myers R, Li Y, Chen Y, Shen X, Fenyk-Melody J, et al. Role of AMP-activated protein kinase in mechanism of metformin action. *Journal of clinical investigation*. 2001;108:1167.

[85] Hawley SA, Boudeau J, Reid JL, Mustard KJ, Udd L, Mäkelä TP, et al. Complexes between the LKB1 tumor suppressor, STRAD α/β and MO25 α/β are upstream kinases in the AMP-activated protein kinase cascade. *Journal of biology*. 2003;2:28.

- [86] Mooney M, Fogarty S, Stevenson C, Gallagher A, Palit P, Hawley S, et al. Mechanisms underlying the metabolic actions of galegine that contribute to weight loss in mice. *British journal of pharmacology*. 2008;153:1669-77.
- [87] Hwang J-T, Kwon DY, Yoon SH. AMP-activated protein kinase: a potential target for the diseases prevention by natural occurring polyphenols. *New Biotechnology*. 2009;26:17-22.
- [88] Lin Y-C, Hung C-M, Tsai J-C, Lee J-C, Chen Y-LS, Wei C-W, et al. Hispidulin potently inhibits human glioblastoma multiforme cells through activation of AMP-activated protein kinase (AMPK). *Journal of agricultural and food chemistry*. 2010;58:9511-7.
- [89] Turner N, Li J-Y, Gosby A, To SW, Cheng Z, Miyoshi H, et al. Berberine and Its More biologically available derivative, dihydroberberine, inhibit mitochondrial respiratory complex IA mechanism for the action of berberine to activate AMP-activated protein kinase and improve insulin action. *Diabetes*. 2008;57:1414-8.
- [90] Gledhill JR, Montgomery MG, Leslie AG, Walker JE. Mechanism of inhibition of bovine F1-ATPase by resveratrol and related polyphenols. *Proceedings of the National Academy of Sciences*. 2007;104:13632-7.
- [91] Musi N, Goodyear L. AMP-activated protein kinase and muscle glucose uptake. *Acta physiologica scandinavica*. 2003;178:337-45.
- [92] Zhang BB, Zhou G, Li C. AMPK: an emerging drug target for diabetes and the metabolic syndrome. *Cell metabolism*. 2009;9:407-16.
- [93] Fogarty S, Hardie D. Development of protein kinase activators: AMPK as a target in metabolic disorders and cancer. *Biochimica et Biophysica Acta (BBA)- Proteins and Proteomics*. 2010;1804:581-91.

- [94] Göransson O, McBride A, Hawley SA, Ross FA, Shpiro N, Foretz M, et al. Mechanism of action of A-769662, a valuable tool for activation of AMP-activated protein kinase. *Journal of Biological Chemistry*. 2007;282:32549-60.
- [95] Barsh GS, Farooqi IS, O'Rahilly S. Genetics of body-weight regulation. *Nature*. 2000;404:644-51.
- [96] Comuzzie AG, Allison DB. The search for human obesity genes. *Science*. 1998;280:1374-7.
- [97] Marti A, Martinez-González MA, Martinez JA. Interaction between genes and lifestyle factors on obesity. *Proceedings of the nutrition society*. 2008;67:1-8.
- [98] Guan T-j, Qin F-j, Du J-h, Geng L, Zhang Y-y, Li M. AICAR inhibits proliferation and induced S-phase arrest, and promotes apoptosis in CaSki cells. *Acta Pharmacologica Sinica*. 2007;28:1984-90.
- [99] Jose C, Hébert-Chatelain E, Bellance N, Larendra A, Su M, Nouette-Gaulain K, et al. AICAR inhibits cancer cell growth and triggers cell-type distinct effects on OXPHOS biogenesis, oxidative stress and Akt activation. *Biochimica et Biophysica Acta (BBA)-Bioenergetics*. 2011;1807:707-18.
- [100] Zhuang Y, Miskimins WK. Cell cycle arrest in Metformin treated breast cancer cells involves activation of AMPK, downregulation of cyclin D1, and requires p27Kip1 or p21Cip1. *Journal of molecular signaling*. 2008;3:18.
- [101] Imamura K, Ogura T, Kishimoto A, Kaminishi M, Esumi H. Cell cycle regulation via p53 phosphorylation by a 5'-AMP activated protein kinase activator, 5-aminoimidazole-4-carboxamide-1- β -D-ribofuranoside, in a human hepatocellular carcinoma cell line. *Biochemical and biophysical research communications*. 2001;287:562-7.
- [102] Wulffele M, Kooy A, Lehert P, Bets D, Ogterop J, Burg B, et al. Effects of

short-term treatment with metformin on serum concentrations of homocysteine, folate and vitamin B12 in type 2 diabetes mellitus: a randomized, placebo-controlled trial. *Journal of internal medicine*. 2003;254:455-63.

[103] Andres E, Noel E, Goichot B. Metformin-associated vitamin B12 deficiency. *Archives of internal medicine*. 2002;162:2251-2.

[104] Liu KW, Dai LK, Jean W. Metformin-related vitamin B12 deficiency. Age and ageing. 2006;35:200-1.

[105] De Jager J, Kooy A, Lehert P, Wulffelé MG, Van der Kolk J, Bets D, et al. Long term treatment with metformin in patients with type 2 diabetes and risk of vitamin B-12 deficiency: randomised placebo controlled trial. *BmJ*. 2010;340.

[106] Ting RZ-W, Szeto CC, Chan MH-M, Ma KK, Chow KM. Risk factors of vitamin B12 deficiency in patients receiving metformin. *Archives of internal medicine*. 2006;166:1975-9.

[107] Adams J, Chen ZP, Van Denderen BJ, Morton CJ, Parker MW, Witters LA, et al. Intrasteric control of AMPK via the γ 1 subunit AMP allosteric regulatory site. *Protein science*. 2004;13:155-65.

[108] Marsin A, Bertrand L, Rider M, Deprez J, Beauloye C, Vincent MF, et al. Phosphorylation and activation of heart PFK-2 by AMPK has a role in the stimulation of glycolysis during ischaemia. *Current biology*. 2000;10:1247-55.

[109] Hardie DG, Hawley SA. AMP-activated protein kinase: the energy charge hypothesis revisited. *Bioessays*. 2001;23:1112-9.

<국문 초록>

비만과 대사성 질환의 주요 원인으로 불리는 인슐린 저항성은 제 2 형 당뇨병, 고지혈증, 고혈당증, 고콜레스테롤증, 동맥경화 및 심혈관 질환 등에 밀접한 연관관계를 지닌다. 특히 지방대사물질은 인슐린 저항성의 발생과 진행에 있어 중요한 역할을 하기 때문에 지방대사의 조절은 인슐린 저항성과 대사성 질환의 개선에 매우 중요하다.

본 연구를 수행하기 위하여 *Cleistocalyx operculatus* 라는 작물의 추출물에서 PPAR γ 의 활성을 증가시키는 단일화합물 2',4'-dihydroxy-6'-methoxy-3',5'-dimethylchalcone (DMC) 를 동정하였다. *C. operculatus* 는 동남아시아 전역에 널리 퍼져 자생하는 작물로 현지에서는 그 추출물로 열의 내림과 고혈당증에 치료제로 사용되고 있다. DMC 가 종양생성의 억제와 항산화, 항염증반응에 탁월한 효과가 있다는 것은 이미 여러 편의 논문으로써 발표된 바 있지만, 당뇨와 대사성질환의 개선부분에는 아직까지 밝혀진 바가 없었다.

먼저, PPAR γ 의 전사활성 능력을 살펴보았다. 기존에 사용되는 rosiglitazone 가 비교해 볼 때, 전사활성 능력은 절반 정도의 활성을

보였고 PPAR γ 의 작용제 결합부위와의 직접적인 결합의 정도에서도 10 배정도 낮은 결과를 보였지만 지방산의 산화에서는 더 높은 활성을 나타내는 특징이 있었다. 흥미롭게도 rosiglitazone 과는 다르게 지방세포 분화를 억제하는 작용이 있어 그 가치가 있다고 기대된다.

또한 DMC 는 PPAR γ 와 더불어 당뇨 및 대사성 질환의 주요한 표적중의 하나인 AMP-dependent protein kinase (AMPK) 의 인산화를 증가시킨다. 기존에 보고된 AICAR, metformin 과 비교하였을 때 두 약제보다 훨씬 낮은 농도에서도 활성을 나타냄을 확인할 수 있었고 AMPK 와의 직접적인 결합의 세기도 AMP 보다 더 강한 것을 확인 할 수 있었다.

다음으로, 12 주간 고지방사료를 식이 함으로써 비만을 유도한 동물모델에 2 주간 경구투여 하는 방식을 이용하여 DMC 가 인슐린 저항성 및 제 2 형 당뇨에 미치는 영향을 관찰하였다. 비록 DMC 가 비교군으로 사용한 pioglitazone 만큼의 인슐린 저항성을 개선하는 효과를 확인하기는 어려웠으나 체중증가를 유발하지 않았고, 지방조직의 감소를 유도하였다는 점에서 큰 의의가 있었다. 이들 결과를 종합해 볼 때,

DMC 는 비만 등의 다양한 부작용 없이 지방대사 및 인슐린 저항성을 개선하는데 큰 도움을 줄 것으로 기대된다.

주요어 : DMC, 인슐린 저항성, 제 2형 당뇨, TZD, PPAR γ , AMPK

학번 : 2009-30616